ORIGINAL ARTICLE

lajss.org Latin American Journal of Solids and Structures

www.lajss.org

An Adaptive Refinement Strategy Based on Equilibrated Flux Error Estimation for Elliptic Problems in Conforming Finite Element Settings

Philippe R. B. Devloo [a], **Ricardo J. Hancco Ancori** [b*], **Eliseo D. Velásquez Condori** [b], **Roger E. Mestas Chavez** [b], **Fermín F. Mamani Condori** [b]

[a] Faculdade de Engenharia Civil, Arquitetura e Urbanismo, Universidade Estadual de Campinas, FECFAU/UNICAMP, Campinas, SP, Brazil. Email: phil@unicamp.br

[b] Departamento Académico de Matemáticas, Universidad Nacional de San Agustín de Arequipa, DAM/UNSA, Arequipa, Perú. Email: rhanccoan@unsa.edu.pe, evelasquezcon@unsa.edu.pe, rmestasc@unsa.edu.pe, fmamani5@unsa.edu.pe

* Corresponding author

https://doi.org/10.1590/1679-7825/e8860

Abstract

In this work we demonstrate the effectiveness of an a-posteriori error estimator based on the Prager Synge theorem for a wide range of problems: smooth problem, problem with a steep gradient, problem with a boundary condition induced singularity, problem with varying conductivity. A very simple but innovative strategy is presented for deciding on h or p adaptivity. Exponential convergence rates were obtained for all test problems. The reconstruction of $H(div)$ compatible functions is applied to meshes with hanging nodes. We believe this work represents an important step towards a cost effective hp -adaptive strategy with a posteriori error estimation.

Keywords

Adaptive mesh refinement, hp -Adaptivity, Adaptive finite element method, Error estimation, Flux reconstruction, Automatic error control.

Graphical Abstract

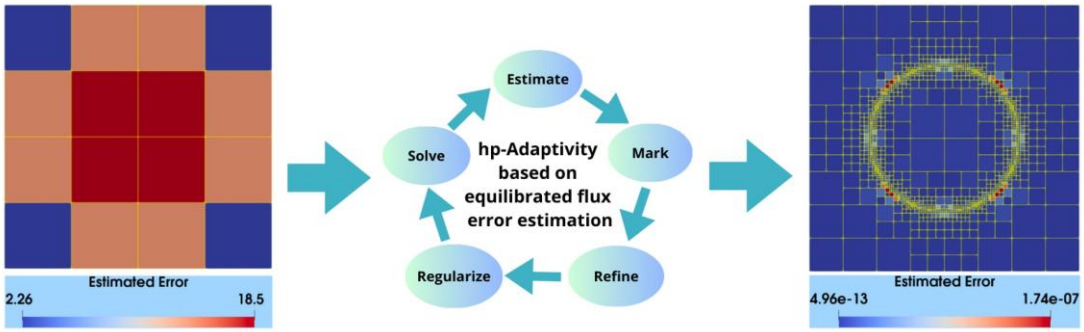

Received October 02, 2025. In revised form October 10, 2025. Accepted November 07, 2025. Available online November 12, 2025.
https://doi.org/10.1590/1679-7825/e8860

1 INTRODUCTION

The convergence rate (in the energy norm) of traditional finite element approximations are suboptimal in the presence of singularities. If prescribed accuracies are required, strongly graded meshes must be used resulting in a substantial increase in the number of degrees of freedom of the global system of equations.

The hp -Finite Element Method (hp -FEM) generalizes FEM by allowing independent adjustment of both mesh size (h) and polynomial degree (p) within each element. Pioneering research by Babuska et al. (Gui and Babuska, 1986; Guo and Babuska, 1986a,b) established that hp -FEM achieves exponentially fast convergence when proper hp -adaptivity is applied. This approach concentrates degrees of freedom in regions of interest by strategically combining localized h -refinement (dividing elements into smaller ones) and p -enrichment (increasing the polynomial approximation order within an element). In essence, hp -adaptivity provides an efficient approach to decreasing the computational effort involved in achieving high-resolution simulations.

Since then, various hp -adaptive strategy approaches have been proposed, primarily driven by localized a posteriori error estimation metrics. For instance, works in Demkowicz et al. (2002) and Rachowicz et al. (2006) are based on minimizing the global interpolation error, while approaches by Ainsworth and Senior (1998); Dorfler and Heuveline (2007), and Heuveline and Rannacher (2003) rely on the local regularity of the exact solution, determined by solving local boundary value problems. Furthermore, the approaches by Eibner and Melenk (2007) and Houston and Süli (2005) are based on the analyticity estimate of the exact solution. Incorporating knowledge of the underlying physical behavior of the problem enhances decision- making and can lead to effective hp -refinement efficiency (Ainsworth and Senior, 1999). For conforming hp -FEM approximations in elliptic problems, in Mitchell and McClain (2014), several hp -adaptive strategies are comprehensively summarized, and the results of numerical experiment designed to evaluate their performance are presented.

A properly designed a posteriori error estimator provides effective information about the error in a specified norm or in a functional of interest, both locally and globally. The Prager and Synge hypercircle method (Prager and Synge, 1947), originally developed for elasticity problems, detailed also in Synge (1957) and Bertrand et al. (2020), served as a foundational inspiration for a posteriori error estimators that utilize equilibrated flux reconstruction in Galerkin approximations for elliptic problems. However, Ladeveze and Leguillon (1983) pioneered this type of error estimation, developing a local equilibrated flux reconstruction technique. By employing the partition of unity, their method allows the construction of an equilibrated flux to be reduced to localized, vertex patch-based calculations. For computational efficiency, patch-based reconstruction can be advantageously employed over global reconstruction techniques.

Unlike residual-based error estimators (Verfiirth, 2013), whose reliability constants are typically unknown and problem-dependent, equilibrated flux a posteriori error estimators offer the distinct advantage of providing error upper bounds with a constant of one. Both types of estimators satisfy local efficiency, meaning the error estimate also represents local lower bounds of the error, up to a generic constant. Another appealing property of equilibrated flux a posteriori error estimators (first revealed for Braess et al. (2009) in the conforming finite element setting) is that the error estimator is polynomial-degree robustness. This signifies that the generic constant in the local error lower bound is independent of the polynomial degree, depending solely on the shape-regularity parameter of the underlying mesh. The polynomial-degree robustness does not hold for residual-based estimators, as shown by Melenk and Wohlmuth (2001). Recent overviews providing insights into the state-of-the-art and perspectives concerning a posteriori error estimation and adaptivity can be found in, e.g., Chamoin and Legoll (2023); Becker et al. (2024) and Bringmann et al. (2024).

Vohralík et al. (Ern and Vohralík, 2015; Dolejsi et al., 2016) introduced a polynomial-degree-robust equilibrated flux a posteriori error estimator. This estimator is applicable to conforming, non-conforming, discontinuous Galerkin, and mixed finite element approximations within a unified framework for Poisson problems. Its design relies on the local reconstruction of an equilibrated flux by solving patch-wise problems using a mixed finite element method. Furthermore, Dolejsi et al. (2016) details numerical assessments of hp -adaptive strategies driven by this estimator, employing the interior penalty Discontinuous Galerkin method. Building on these developments, Daniel et al. (2018) proposed an hp -adaptive strategy for H^1 -conforming finite element approximations on conforming simplicial meshes, where the hp -decision is made using two local primal solves on selected patches.

We have not identified any documented computational implementations of hp -adaptive algorithms in the literature that are guided by the generic Vohralík et al. estimator and applied to H^1 -conforming finite element approximations on meshes with hanging nodes. The computational implementation for this scenario inherently presents challenges, including the maintenance of continuity at element interfaces and solving mixed finite element formulations

localized to patches, particularly on non-conforming meshes characterized by elements of various refinement levels and a heterogeneous distribution of polynomial degrees.

In the present work, we focus on the diffusion problem

$$\begin{aligned} -\nabla\cdot\ A\nabla u\ &= f,\ \text{in}\ \Omega \\ u &= 0,\ \text{on}\ \partial\Omega \end{aligned} \tag{1}$$

where $\Omega\subset\mathbb{R}^2$ is a polygonal domain (open, bounded and connected set) with a Lipschitz boundary; A is a symmetric positive definite tensor, and piecewise constant with respect to the decomposition $\overline{\Omega}=\bigcup_{i=1}^{n}\overline{\Omega}_i$, where each subdomain $\Omega_i,\ i=1,...,n$, is open and polygonal; and $f\in L^2(\Omega)$. Our primary goal is to extend the generic error estimator from Ern and Vohralík (2015) to address the diffusion problem (1) and to propose a simple, cost-effective hp-adaptive refinement strategy for H^1-conforming Finite Element approximations on both quadrilateral and triangular meshes, which may be non-conforming.

Broadly, h-adaptivity is employed for an element when its estimated residual and flux errors are both significant. Meanwhile, p-adaptivity is chosen when the element's estimated flux or residual error is low. When dealing with problems featuring point singularities, prior knowledge of their locations dictates the so application of h-refinement to elements directly contacting these singular points.

The structure of this manuscript is as follows. Section 3 extends specific constructs and properties, initially developed for conforming meshes, to nonconforming mesh settings. Section 4 outlines the equilibrated flux reconstruction and the a posteriori error estimator based on equilibrated flux, encompassing both conforming and nonconforming meshes. The hp-adaptive refinement strategy proposed in this work is outlined in Section 5. Results from numerical experiments on five benchmark problems are presented in Section 6. Section 7 explores the sensitivity of the algorithm with respect to variations in its parameters. Finally, conclusions are provided in Section 8.

All numerical experiments were conducted with the assistance of the NeoPZ framework (Devloo, 1997), a multi-purpose Finite Element platform developed entirely in C++ and built upon an object-oriented architectural design.

2 NOTATIONS AND PRELIMINARIES

Let $\mathcal{T}_h$ be a partition (triangular or quadrilateral mesh) of a polygonal domain $\Omega\subset\mathbb{R}^2$, composed of closed elements, generally denoted by K, whose interiors are pairwise disjoint. The coarseness of the mesh is represented by the largest diameter across its elements, which is denoted by h. We are interested in triangular or affine quadrilateral meshes, without any limitations on the hanging sides and with a heterogeneous polynomial degree distribution.

The parametric (master) elements are $\hat{K}=\left\{(x,y):0\le x,\ y\le 1,\ x+y\le 1\right\}$ or $\hat{K}=\left\{(x,y):-1\le x,\ y\le 1\right\}$

Given an element K, let $x_K:\hat{K}\to K$ be the standard geometric map.

The space of square integrable functions (Lebesgue space) is denoted by $L^2(\Omega)=\left\{f:\int_\Omega |f|^2\,d\Omega<\infty\right\}$ and equipped with the usual norm $\|\cdot\|$ defined by $\|f\|^2=\int_\Omega f^2\,d\Omega$ and inner product $(f,\ g)=\int_\Omega fg\,d\Omega$. The Sobolev space of functions whose first-order weak derivatives are square-integrable

$$H^1(\Omega)=\left\{v\in L^2(\Omega):\ D^\alpha v\in L^2(\Omega)\ \forall\alpha,\ |\alpha|\le 1\right\} \tag{2}$$

is equipped with the semi norm $|\cdot|_1$ and norm $\|\cdot\|_1$ defined by $|v|_1^2=\int_\Omega \nabla v\cdot\nabla v\,d\Omega$ and $\|v\|_1^2=\|v\|^2+|v|_1^2$ respectively.

Another space of interest is $\boldsymbol{H}\left(\mathrm{div},\Omega\right)=\left\{\boldsymbol{q}:\boldsymbol{q}\in\left[L^2\left(\Omega\right)\right]^2,\nabla\cdot\boldsymbol{q}\in L^2\left(\Omega\right)\right\}$. The geometric map induces isomorphisms: $\mathcal{F}_K:H^1\left(\hat{K}\right)\rightarrow H^1\left(K\right)$, given by $\mathcal{F}_K\left(\hat{v}\right)=\hat{v}\circ x_K^{-1}$, and the well-known Piola's transformation $\mathcal{F}_K^{\mathrm{div}}:\boldsymbol{H}\left(\mathrm{div};\hat{K}\right)\rightarrow\boldsymbol{H}\left(\mathrm{div};K\right)$.

For an integer $p\geq 0$, let $\mathbb{Q}_p\left(\hat{K}\right)$ (respectively, $\mathbb{P}_p\left(\hat{K}\right)$) represent the space of polynomial functions of maximum degree p in each variable (respectively, of total degree p) on the quadrilateral (respectively, triangular) master element $\hat{K}$. Henceforth, $\mathbb{S}_p\left(\hat{K}\right)$ will represent $\mathbb{Q}_p\left(\hat{K}\right)$ or $\mathbb{P}_p\left(\hat{K}\right)$ according to whether the master element is quadrilateral or triangular, respectively.

Given a polynomial-degree distribution $\mathbf{p}=\left(p_K\right)_{K\in\mathcal{T}_h}$, for each element $K\in\mathcal{T}_h$, consider the polynomial space

$$\mathbb{S}_{p_K}\left(K\right)=\left\{v:v=\mathcal{F}_K\left(\hat{v}\right),\hat{v}\in\mathbb{S}_{p_K}\left(\hat{K}\right)\right\} \tag{3}$$

then the conforming *hp*-finite element space can now be defined as

$$U_h^{\mathbf{p}}=\left\{v\in C^0\left(\Omega\right):v\big|_K\in\mathbb{S}_{p_K}\left(K\right),\forall K\in\mathcal{T}_h\right\}\cap H_0^1\left(\Omega\right) \tag{4}$$

Each space $U_h^{\mathbf{p}}$ is uniquely determined by a pair made up of mesh and polynomial-degree distribution, and reciprocally.

We consider two subspaces of $\boldsymbol{H}\left(\mathrm{div};\hat{K}\right)$, constituted of vector-valued polynomials. If $\hat{K}$ is quadrilateral, it is considered the classical Raviart-Thomas spaces $\mathbf{RT}_p\left(\hat{K}\right)$, and if $\hat{K}$ is triangle, it is considered the classical Brezzi-Douglas-Marini spaces $\mathbf{BDM}_p\left(\hat{K}\right)$, see Ervin (2012). Henceforth, let's represent any of these classical spaces with $\mathbf{M}_p\left(\hat{K}\right)$, depending on the type of master element involved. Also, be

$$\mathbf{M}_p\left(\hat{K}\right)=\left\{v:v=\mathcal{F}_K^{\mathrm{div}}\left(\hat{v}\right),\hat{v}\in M_p\left(\hat{K}\right)\right\} \tag{5}$$

For mixed finite element formulations, the following pair (primal and dual) $hp-$ adaptive spaces are also of interest:

$$V_h^{\mathbf{p}}=\left\{v\in L^2\left(\Omega\right):v\big|_K\in\mathbb{S}_{p_K}\left(K\right),\forall K\in\mathcal{T}_h\right\} \tag{6}$$

and

$$\mathbf{M}_h^{\mathbf{p}}=\left\{v\in H\left(\mathrm{div};\Omega\right):v\big|_K\in M_{p_K}\left(K\right),\forall K\in\mathcal{T}_h\right\} \tag{7}$$

It is well-established that properly balancing the $\boldsymbol{H}\left(\mathrm{div};\Omega\right)-L^2\left(\Omega\right)$ pairs of mixed finite element spaces is of critical importance (De Siqueira et al., 2013; Farias et al., 2017; Devloo et al., 2016).

3 TWO DIMENSIONAL NON-CONFORMAL MESHES

In the two-dimensional case, it is essential to recall that a node in a mesh is called a hanging node when it belongs to the edge of a mesh element without coinciding with any of its vertices. A node not designated as a hanging node is referred to as a free node. A mesh is conforming when it has no hanging nodes; otherwise, it is said to be non-conforming. Equivalently, a mesh is conforming when the non-empty intersection of two distinct elements results in a common node or edge.

In this and the subsequent sections, $\mathcal{T}_h$ denotes either a quadrilateral or triangular mesh, which may be conforming or non-conforming.

Definition 1. The hat function associated with a free node $\boldsymbol{a}$ of $\mathcal{T}_h$, is a continuous function

$\psi^{\boldsymbol{a}} : \Omega \to \mathbb{R}$

such that $\psi^a\big|_K$ belongs to $\mathbb{S}_1\left(K\right)$ for each $K \in \mathcal{T}_h$, and it has a value of 1 at node $\boldsymbol{a}$ and vanishes at all other free nodes of $\mathcal{T}_h$.

Since each function in $\mathbb{S}_1\left(K\right)$, is uniquely determined by its values at the vertices of K, each free node of $\mathcal{T}_h$ has a unique associated hat function. See Figures 1 and 3.

Definition 2. The patch, $\omega_{\boldsymbol{a}}$, associated with a free node $\boldsymbol{a}$ of $\mathcal{T}_h$, is the collection of elements whose interior is contained within the support of the hat function associated with that node.

Definition 2 is illustrated in Figures 1 and 2.

Definition 3. A mesh is k -irregular if it has at least one edge containing a number of k hanging nodes.

According to the above definition, a conformal mesh is a 0 -irregular mesh. Therefore, a conformal mesh is also referred to as a regular mesh.

Higher values of k can result in patches with more complex structures, mainly an increase in the number of elements they comprise, see Figures 1 and 2, which in practice implies greater computational complexity. Moreover, experience has shown that the quality of the gradient reconstruction degrades when $k>1$. For this reason, in this article, we work with meshes that are up to 1-irregular.

Lemma 1. (Partition unity property) Let $\mathcal{T}_{h_i}^i$ be a mesh obtained in the i-th iteration by applying successive adaptive $h-$ refinements with arbitrary element selection in each iteration, starting from an initial conforming triangular or quadrilateral mesh $\mathcal{T}_{h_0}^0$, where the $h-$ refinement of an element consists of dividing it into four sub-elements using line segments connecting the midpoints of its sides. Then, for each $i \geq 0$, the sum of the hat functions corresponding to $\mathcal{T}_{h_i}^i$ is equal to 1.

Proof. For the mesh $\mathcal{T}_{h_i}^i$, let $\mathcal{N}_i$ denote the set of free nodes, $\psi_i^{\boldsymbol{a}}$ (where $\boldsymbol{a} \in \mathcal{N}_i$) the respective hat function, and $S_i = \sum_{a \in \mathcal{N}_i} \psi_i^{\boldsymbol{a}}$ (the sum of all hat functions associated with $\mathcal{T}_{h_i}^i$).

Due to the polynomial structure of the hat functions over each element of $\mathcal{T}_{h_i}^i$, if S_i assumes a constant value at all vertices of the element $K \in \mathcal{T}_h$, then it holds the same value over the entire element.

The proof will proceed by induction on i. In the case $i = 0$, the property is satisfied due to the conforming nature of the mesh.

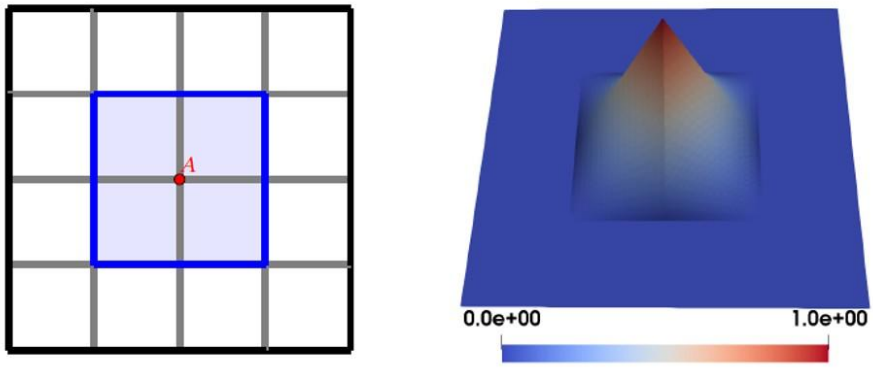

Figure 1. A patch associated to a node A in a 0-irregular mesh (left) and its hat function (right).

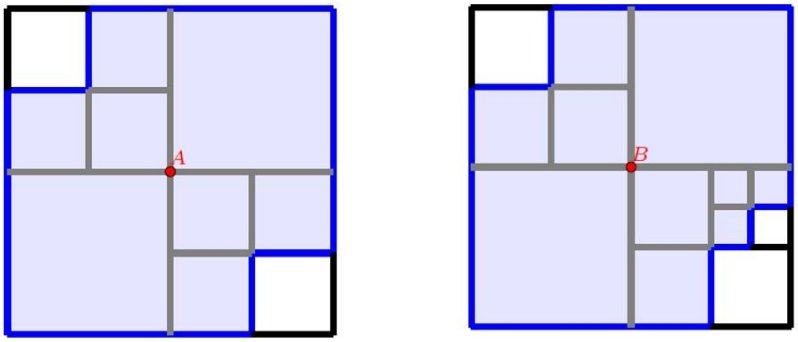

Figure 2. Patch of node A in a 1-irregular mesh (left) and of node B in a 2-irregular mesh (right).

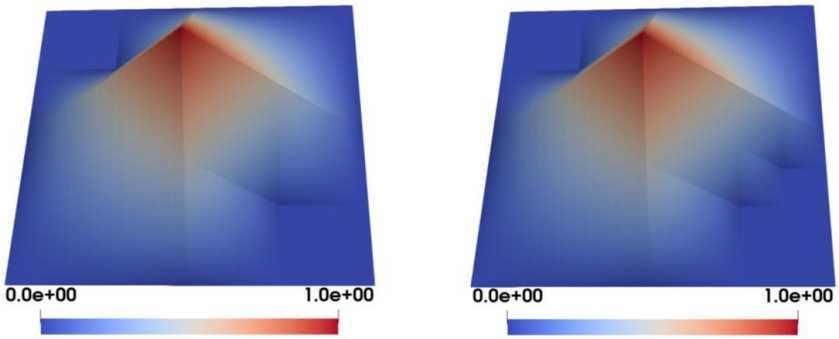

Figure 3. Hat functions of the patches associated with nodes A (left) and B (right) of Figure 2.

Assume that $S_i = 1$ is true for some $i = k$, $k \geq 0$. Note that $\mathcal{N}_k \subset \mathcal{N}_{k+1}$. For each $K \in \mathcal{T}_{h_k}^k \cap \mathcal{T}_{h_{k+1}}^{k+1}$, it holds that $\psi_k^{\boldsymbol{a}}\big|_K = \psi_{k+1}^{\boldsymbol{a}}\big|_K$ for $a \in \mathcal{N}_k$, and $\psi_{k+1}^{\boldsymbol{a}}\big|_K = 0$ for $\boldsymbol{a} \in \mathcal{N}_{k+1} \setminus \mathcal{N}_k$. Consequently, we obtain

$$S_{k+1}\big|_K = \sum_{a \in \mathcal{N}_{k+1}} \psi_{k+1}^{\boldsymbol{a}}\big|_K = \sum_{a \in \mathcal{N}_k} \psi_{k+1}^{\boldsymbol{a}}\big|_K = S_k\big|_K = 1 \tag{8}$$

Now, let's take $K \in \mathcal{T}_{h_{k+1}}^{k+1} \setminus \mathcal{T}_{h_k}^k$ and let b be a vertex of this. If $b \in \mathcal{N}_{k+1}$, it holds that $S_{k+1}(b) = \psi_{k+1}^a(b) = 1$. When b is a hanging node of $\mathcal{T}_{h_{k+1}}^{k+1}$, it belong to boundary of some element of $\mathcal{T}_{h_k}^k \cap \mathcal{T}_{h_{k+1}}^{k+1}$, and by (8) we also conclude that $S_{k+1}(b) = 1$.

4 EQUILIBRATED FLUX A POSTERIORI ERROR ESTIMATE

The weak primal formulation of problem (1) is given by: Find $u \in H_0^1(\Omega)$ such that

$$\left(A\nabla u, \nabla v\right) = \left(f, v\right) \ \forall v \in H_0^1(\Omega) \tag{9}$$

and the discretized weak primal formulation of problem (1) is given by: Find $u_h \in U_h^{\mathrm{p}}$ such that

$$\left(A\nabla u_h, \nabla v_h\right) = \left(f, v_h\right) \ \forall v_h \in U_h^{\mathrm{p}} \tag{10}$$

Any function $\boldsymbol{\sigma}$ in $\boldsymbol{H}(\mathrm{div}, \Omega)$ constructed from u_h such that,

$$\left(\nabla \cdot \boldsymbol{\sigma}, 1\right)_K = \left(f, 1\right)_K \qquad \forall K \in \mathcal{T}_h \tag{11}$$

we will call the reconstructed equilibrated flux.

4.1 The Generalized Prager-Synge identity

Theorem 1. Let $u \in H_0^1(\Omega)$ be the solution of (9) and $\boldsymbol{\sigma} \in \boldsymbol{H}\left(\mathrm{div}, \Omega\right)$ satisfying the equilibrium equation $\mathrm{div}\, \boldsymbol{\sigma} = f$. Then

$$\left|\left| A^{\frac{1}{2}} \nabla u - A^{\frac{1}{2}} \nabla v \right|\right|^2 + \left|\left| A^{-\frac{1}{2}} \boldsymbol{\sigma} + A^{\frac{1}{2}} \nabla u \right|\right|^2 = \left|\left| A^{-\frac{1}{2}} \boldsymbol{\sigma} + A^{\frac{1}{2}} \nabla v \right|\right|^2, \tag{12}$$

for all $v \in H_0^1(\Omega)$.

Proof.

$$\left|\left| A^{-\frac{1}{2}} \boldsymbol{\sigma} + A^{\frac{1}{2}} \nabla v \right|\right|^2 = \left|\left| A^{\frac{1}{2}} \nabla v - A^{\frac{1}{2}} \nabla u \right|\right|^2 + \left|\left| A^{-\frac{1}{2}} \boldsymbol{\sigma} + A^{\frac{1}{2}} \nabla u \right|\right|^2 + 2\left(A^{\frac{1}{2}} \nabla v - A^{\frac{1}{2}} \nabla u, A^{-\frac{1}{2}} \boldsymbol{\sigma} + A^{\frac{1}{2}} \nabla u\right) \tag{13}$$

In the previous equality, the third term on the right side is zero, since by property $A^{\frac{1}{2}}$ is symmetric, and

$$\int_\Omega \left(\nabla v - \nabla u\right)^t \left(A^{\frac{1}{2}}\right)^t \left(A^{-\frac{1}{2}} \boldsymbol{\sigma} + A^{\frac{1}{2}} \nabla u\right) d\Omega = \int_\Omega \left(\nabla v - \nabla u\right)^t \left(\boldsymbol{\sigma} + A\nabla u\right) d\Omega = \left(\nabla v - \nabla u, \boldsymbol{\sigma} + A\nabla u\right) = 0. \tag{14}$$

The last equality is obtained by applying Green's theorem on $H_0^1(\Omega) \times \boldsymbol{H}(\mathrm{div}, \Omega)$.

Taking $v = u_h$ and $\boldsymbol{\sigma} = \boldsymbol{\sigma}_h$ where u_h is the solution of (10) and $\boldsymbol{\sigma}_h$ is any equilibrated flux reconstructed, a direct application of Prager-Synge identity gives an a posteriori error estimator with constant one

$$\left|\left| A^{\frac{1}{2}} \nabla u - A^{\frac{1}{2}} \nabla u_h \right|\right|^2 \leq \left|\left| A^{-\frac{1}{2}} \boldsymbol{\sigma}_h + A^{\frac{1}{2}} \nabla u_h \right|\right|^2 \tag{15}$$

4.2 Flux reconstruction for conforming and nonconforming meshes

Let $(\mathbf{M}_h, V_h) \in \boldsymbol{H}(\mathrm{div},\Omega) \times L^2(\Omega)$ be a pair of mixed finite element spaces, and let $\mathbf{M}_h^{\boldsymbol{a}}$ and $V_h^{\boldsymbol{a}}$ denote their respective restrictions to the patch $\omega_{\boldsymbol{a}}$. In addition, let $\mathcal{V}_h$ be the set of free nodes of $\mathcal{T}_h$, and their respective subsets of interior nodes and border nodes $\mathcal{V}_h^{\mathrm{int}}$ and $\mathcal{V}_h^{\mathrm{ext}}$.

The following definition represents an extension of Definition 3.1 in Daniel et al. (2018), formulated to enable equilibrated flux reconstruction in the context of diffusion problems such as (1).

Definition 4 (Equilibrated flux reconstruction $\boldsymbol{\sigma}_h$) Let u_h solve (10). For each $\boldsymbol{a} \in \mathcal{V}_h$, prescribe $\boldsymbol{\varsigma}_h^{\boldsymbol{a}} \in \mathbf{M}_h^{\boldsymbol{a}}$ and $\overline{r}_h^{\boldsymbol{a}} \in V_h^{\boldsymbol{a}}$ by solving

$$\left(A^{-1}\varsigma_h^{\boldsymbol{a}}, \mathbf{v}_h\right)_{\omega_{\boldsymbol{a}}} - \left(\overline{r}_h^{\boldsymbol{a}}, \nabla \cdot \mathbf{v}_h\right)_{\omega_{\boldsymbol{a}}} = -\left(\psi_{\boldsymbol{a}} \nabla u_h, \mathbf{v}_h\right)_{\omega_{\boldsymbol{a}}} \quad \forall \mathbf{v}_h \in \mathbf{M}_h^{\boldsymbol{a}} \tag{16}$$

$$\left(\nabla \cdot \varsigma_h^{\boldsymbol{a}}, q_h\right)_{\omega_{\boldsymbol{a}}} = \left(\psi_{\boldsymbol{a}} f - \nabla \psi_{\boldsymbol{a}} \cdot A \nabla u_h, q_h\right)_{\omega_{\boldsymbol{a}}} \quad \forall q_h \in V_h^{\boldsymbol{a}} \tag{17}$$

with the spaces

$$\mathbf{V}_h^{\boldsymbol{a}} \coloneqq \left\{\mathbf{v}_h \in \mathbf{V}_h(\omega_{\boldsymbol{a}}) : \mathbf{v}_h \cdot n_{\omega_{\boldsymbol{a}}} = 0 \text{ on } \partial\omega_{\boldsymbol{a}}\right\},\ \boldsymbol{a} \in \mathcal{V}_h^{int} \tag{18}$$

$$S_h^{\boldsymbol{a}} \coloneqq \left\{q_h \in S_h(\omega_{\boldsymbol{a}}) : (q_h, 1)_{\omega_{\boldsymbol{a}}} = 0\right\},\ \boldsymbol{a} \in \mathcal{V}_h^{int} \tag{19}$$

$$\mathbf{V}_h^{\boldsymbol{a}} \coloneqq \left\{\mathbf{v}_h \in \mathbf{V}_h(\omega_{\boldsymbol{a}}) : \mathbf{v}_h \cdot n_{\omega_{\boldsymbol{a}}} = 0 \text{ on } \partial\omega_{\boldsymbol{a}} \setminus \partial\Omega\right\},\ \boldsymbol{a} \in \mathcal{V}_h^{ext} \tag{20}$$

$$S_h^{\boldsymbol{a}} \coloneqq S_h(\omega_{\boldsymbol{a}}),\ \boldsymbol{a} \in \mathcal{V}_h^{ext} \tag{21}$$

Then, set

$$\boldsymbol{\sigma}_h \coloneqq \sum_{\boldsymbol{a} \in \mathcal{V}_h} \varsigma_h^{\boldsymbol{a}} \tag{22}$$

Unlike the equilibrated flux reconstruction proposed in Dolejsi et al. (2016) and Daniel et al. (2018), which imposes adjustments on both patch meshes and their corresponding polynomial degree distributions, our approach does not require such local constraints.

4.3 A posteriori error estimate

The purpose of an a posteriori error estimates is to establish bounds on the error between the obtained numerical approximation and the exact, yet unknown, solution. This computation is feasible in practice after the approximate solution is available.

The following theorem is an extended version of Theorem 3.3 of Earn and Vohralík (2015) to problems with heterogeneous permeability. The demonstration follows the same method as the original theorem's proof, with appropriate adjustments to handle the extended scope.

Theorem 2 Let u the solution of (9) and u_h an arbitrary function in $H^1\left(\mathcal{T}_h\right)$. Let s_h be a potential reconstruction and $\boldsymbol{\sigma}_h$ an equilibrated flux reconstruction. For any $K \in \mathcal{T}_h$, define the residual estimator by

$$\eta_{R,K} \coloneqq \frac{h_K}{\pi C_{A,K}^{\frac{1}{2}}} \left|\left| f - \nabla \cdot \boldsymbol{\sigma}_h \right|\right|_K, \tag{23}$$

where $C_{A,K}$ is the smallest eigenvalue of A on element K; the flux estimator by

$$\eta_{F,K} \coloneqq \left|\left| A^{\frac{1}{2}} \nabla u_h + A^{-\frac{1}{2}} \boldsymbol{\sigma}_h \right|\right|_K \tag{24}$$

and the non-conformity estimator by

$$\eta_{NC,K} \coloneqq \left|\left| A^{\frac{1}{2}} \nabla u_h - A^{\frac{1}{2}} \nabla s_h \right|\right|_K \tag{25}$$

The following upper bound holds:

$$\left|\left| A^{\frac{1}{2}} \nabla u - A^{\frac{1}{2}} \nabla u_h \right|\right|^2 \leq \sum_{K \in \mathcal{T}_h} (\eta_{F,K} + \eta_{R,K})^2 + \sum_{K \in \mathcal{T}_h} \eta_{NC,K}^2. \tag{26}$$

Proof. Consider the broken Sobolev space $H^1(\mathcal{T}_h)$ equipped with the positive semidefinite H^1-broken inner product $(A\nabla\cdot, \nabla\cdot)$, this induces an (auxiliary) inner product on $H_0^1(\Omega)$, constituting an (auxiliary) Hilbert space. Then, applying the Riesz representation theorem to the functional defined on the auxiliary space $(A\nabla u_h, \cdot) : H_0^1(\Omega) \to \mathbb{R}$, there exist one and only one $s \in H_0^1(\Omega)$ such that

$$(A\nabla s, \nabla v) = (A\nabla u_h, \nabla v) \quad \forall v \in H_0^1(\Omega) \tag{27}$$

The continuity of the defined functional is justified from the Cauchy-Schwarz inequality

$$\left| (A\nabla u_h, \nabla v) \right| \leq \| A^{\frac{1}{2}} \nabla u_h \| \| A^{\frac{1}{2}} \nabla v \| \tag{28}$$

From Equation (27) we conclude that the function $s - u_h$ is orthogonal to $H_0^1(\Omega)$ respect to positive semidefinite H^1-broken inner product. By this property we obtain

$$\| A^{\frac{1}{2}} \nabla w - A^{\frac{1}{2}} \nabla u_h \|^2 = \| A^{\frac{1}{2}} \nabla w - A^{\frac{1}{2}} \nabla s \|^2 + \| A^{\frac{1}{2}} \nabla s - A^{\frac{1}{2}} \nabla u_h \|^2 \forall w \in H_0^1(\Omega) \tag{29}$$

and

$$\| A^{\frac{1}{2}} \nabla (s - u_h) \| = \min_{w \in H_0^1(\Omega)} \| A^{\frac{1}{2}} \nabla (w - u_h) \| \tag{30}$$

From (30) we obtain

$$\| A^{\frac{1}{2}} \nabla(s - u_h) \|^2 \leq \| A^{\frac{1}{2}} \nabla(s_h - u_h) \|^2 = \sum_{K \in \mathcal{T}_h} \eta^2_{NC,K} \tag{31}$$

Also, by Riesz representation theorem applied on the auxiliary Hilbert space, for all $v \in H^1_0(\Omega)$ we have

$$\| A^{\frac{1}{2}} \nabla v \| = \sup_{\varphi \in H^1_0(\Omega): \| A^{\frac{1}{2}} \nabla \varphi \| = 1} (A^{\frac{1}{2}} \nabla v, A^{\frac{1}{2}} \nabla \varphi), \tag{32}$$

which together with the Equation (27) gives

$$\| A^{\frac{1}{2}} \nabla(u - s) \| = \sup_{\varphi \in H^1_0(\Omega): \| A^{\frac{1}{2}} \nabla \varphi \| = 1} (A^{\frac{1}{2}} \nabla(u - s), A^{\frac{1}{2}} \nabla \varphi)$$

$$= \sup_{\varphi \in H^1_0(\Omega): \| A^{\frac{1}{2}} \nabla \varphi \| = 1} (A^{\frac{1}{2}} \nabla(u - u_h), A^{\frac{1}{2}} \nabla \varphi). \tag{33}$$

Let $\varphi \in H^1_0(\Omega)$. Using the weak formulation (9) we have

$$\left(A^{\frac{1}{2}} \nabla(u - u_h), A^{\frac{1}{2}} \nabla \varphi\right) = (f, \varphi) - (A^{\frac{1}{2}} \nabla u_h, A^{\frac{1}{2}} \nabla \varphi) \tag{34}$$

then adding and subtracting $\left(A^{-\frac{1}{2}} \sigma_h, A^{\frac{1}{2}} \nabla \varphi\right)$ and using the Green identity, we obtain

$$\left(A^{\frac{1}{2}} \nabla(u - u_h), A^{\frac{1}{2}} \nabla \varphi\right) = (f - \nabla \cdot \boldsymbol{\sigma}_h, \varphi) - \left(A^{\frac{1}{2}} \nabla u_h + A^{-\frac{1}{2}} \boldsymbol{\sigma}_h, A^{\frac{1}{2}} \nabla \varphi\right). \tag{35}$$

The Cauchy-Schwarz inequality gives

$$-\left(A^{\frac{1}{2}} \nabla u_h + A^{-\frac{1}{2}} \boldsymbol{\sigma}_h, A^{\frac{1}{2}} \nabla \varphi\right) \leq \sum_{K \in \mathcal{T}_h} \| A^{\frac{1}{2}} \nabla u_h + A^{-\frac{1}{2}} \boldsymbol{\sigma}_h \|_K \| A^{\frac{1}{2}} \nabla \varphi \|_K \tag{36}$$

$$= \sum_{K \in \mathcal{T}_h} \eta_{F,K} \| A^{\frac{1}{2}} \nabla \varphi \|_K$$

Let φ_K denote the average value of φ over element K. From Poincaré's inequality and the properties of the permeability tensor we obtain

$$\| \varphi - \varphi_K \| \leq \frac{h_K}{\pi C_{A,K}^{\frac{1}{2}}} \| A^{\frac{1}{2}} \nabla \varphi \| \tag{37}$$

which, together the weak flux equilibrium property and the Cauchy-Schwarz inequality gives

$$\begin{aligned}
(f - \nabla \cdot \sigma_h, \varphi) &= \sum_{K \in \mathcal{T}_h} (f - \nabla \cdot \sigma_h, \varphi)_K \\
&= \sum_{K \in \mathcal{T}_h} (f - \nabla \cdot \sigma_h, \varphi - \varphi_K)_K \\
&\leq \sum_{K \in \mathcal{T}_h} \frac{h_K}{\pi C_{A,K}^{\frac{1}{2}}} \| f - \nabla \cdot \sigma_h \|_K \| A^{\frac{1}{2}} \nabla \varphi \|_K \qquad (38) \\
&= \sum_{K \in \mathcal{T}_h} \eta_{R,K} \| A^{\frac{1}{2}} \nabla \varphi \|_K
\end{aligned}$$

Combining (33), (35), (36), (38) and the Cauchy-Schwarz inequality we get

$$\begin{aligned}
\| A^{\frac{1}{2}} \nabla (u - s) \|^2 &= \Big(\sup_{\varphi \in H_0^1(\Omega): \| A^{\frac{1}{2}} \nabla \varphi \| = 1} \Big\{ (f - \nabla \sigma_h, \varphi) - \left(A^{\frac{1}{2}} \nabla u_h + A^{-\frac{1}{2}} \sigma_h, A^{\frac{1}{2}} \nabla \varphi \right) \Big\} \Big)^2 \\
&\leq \Big(\sup_{\varphi \in H_0^1(\Omega): \| A^{\frac{1}{2}} \nabla \varphi \| = 1} \Big\{ \sum_{K \in \mathcal{T}_h} (\eta_{F,K} + \eta_{R,K}) \| A^{\frac{1}{2}} \nabla \varphi \|_K \Big\} \Big)^2 \qquad (39) \\
&\leq \sum_{K \in \mathcal{T}_h} (\eta_{F,K} + \eta_{R,K})^2
\end{aligned}$$

The desired inequality is obtained by combining equation (29) by setting $w = u_h$ and equation (31).

For the H^1-conforming finite element discretization applied to the problem (1), the non-conformity estimator is null, therefore the estimator of Theorem 2 reduces to the following: Let u and u_h be the solutions of (9) and (10) respectively, then

$$\left| \left| A^{\frac{1}{2}} \nabla u - A^{\frac{1}{2}} \nabla u_h \right| \right|^2 \leq \sum_{K \in \mathcal{T}_h} (\eta_{F,K} + \eta_{R,K})^2 \tag{40}$$

4.4 Effectivity index

To evaluate the accuracy of the error estimator under study, the effectivity index is defined as follows:

$$I_{eff} = \frac{\Big(\sum_{K \in \mathcal{T}_h} (\eta_{F,K} + \eta_{R,K})^2 \Big)^{\frac{1}{2}}}{|| A^{\frac{1}{2}} \nabla u - A^{\frac{1}{2}} \nabla u_h ||} \tag{41}$$

5 hp -ADAPTIVE SCHEME

For problems with smooth and sufficiently regular solutions, p -refinement is known to achieve exponential convergence rates of the error with respect to the number of degrees of freedom. However, in regions exhibiting irregularities such as high gradients, abrupt oscillations, or singularities, p -refinement is less efficient when compared to h -refinement (Ainsworth and Oden, 2011; Mitchell and McClain, 2011). The combination of h and p -refinement using an appropriate strategy can result in efficient meshes for the complete range of problems.

In this study, when an element K is selected for refinement, it undergoes either h -adaptivity or p -adaptivity exclusively, this decision is guided by a regularity-based strategy, whereby elements in regions with predicted singularities or low regularity are h -refined, and those in smooth regions are p -refined.

A priori knowledge of the location of point singularities is utilized in problems with re-entrant corners or changes of coefficients. This knowledge informs the initial mesh ($\mathcal{T}_{h_0}^0$) design, placing singularity points as nodes. Consequently, during the adaptive phase, elements possessing a vertex at a singularity are always h -refined.

The hp -adaptive algorithm we employ adheres to a well-known iterative paradigm, where each iteration comprises the following modules (see, e.g., Daniel et al. (2018) and Demkowicz et al. (1985)):

$$\text{SOLVE} \rightarrow \text{ESTIMATE} \rightarrow \text{MARK} \rightarrow \text{REFINE} \rightarrow \text{REGULARIZE}. \tag{42}$$

In terms of finite element spaces, the Algorithm 42 requires as input the initial conforming hp -finite element space $U_{h_0}^{\mathbf{p}_0}$ (defined by mesh $\mathcal{T}_{h_0}^0$ and polynomial-degree distribution $\mathbf{p}_0$), the maximum number of iterations $N+1$, threshold parameters τ_1, τ_2, ρ, the tolerance Tol and where applicable, the prescribed singularity coordinates. Each iteration indexed by i, where $0 \le i \le N$, receives a conforming hp -finite element space $U_{h_i}^{\mathbf{p}_i}$, and yield as output a numerical solution, u_{h_i}, of the conforming hp -finite element formulation: Find $u_{h_i} \in U_{h_i}^{\mathbf{p}_i}$ such that

$$\left(A\nabla u_{h_i}, \nabla v\right) = \left(f, v\right), \tag{43}$$

$\forall v \in U_{h_i}^{\mathbf{p}_i}$; as well as a conforming hp -finite element space $U_{h_{i+1}}^{\mathbf{p}_{i+1}}$, to be used in the next iteration.

Algorithm 1: hp - Adaptive algorithm

Input: Initial mesh $\mathcal{T}_{h_0}^0$, initial polynomial-degree distribution $\mathbf{p}_0$, threshold parameters τ_1, τ_2, ρ, tolerance Tol, number of iterations $N+1$, prescribed singularity coordinates (if applicable).

Output: H^1 -conforming discrete solution u_N

1 Initialize mesh $\mathcal{T} \leftarrow \mathcal{T}_{h_0}^0$

2 Initialize polynomial- degree distribution $\mathbf{p} \leftarrow \mathbf{p}_0$

3 **for** $i = 0$ to N do

4 **Solve:** Compute the FEM solution u_h on mesh $\mathcal{T}$ with polynomial degrees $\mathbf{p}$

5 **Estimate:** Calculate a posteriori error estimates $\eta_{R,K}$, $\eta_{F,K}$ for each element $K \in \mathcal{T}$

6 **Mark:** Mark elements for h or p refinement based on local a posteriori error estimates and, if applicable, a priori singularity locations

7 **Refine:** Apply h - or p -refinement to marked elements to obtain new mesh $\mathcal{T}$ and update polynomial degrees $\mathbf{p}$

8 **Regularize:** Regularize the mesh, enforcing the two on one constraint

end

The hp -adaptivity process is encapsulated in Algorithm 1, and the five associated modules are comprehensively described in the following parts of this section.

5.1 Module SOLVE

Receives the mesh $\mathcal{T}_{h_i}^i$ and an associated polynomial-degree distribution $\mathbf{p}_i$, and returns the solution u_{h_i} of discrete formulation (43).

5.2 Module ESTIMATE

This module take as input $\mathcal{T}_{h_i}^i$, $\mathbf{p}_i$ and the solution u_{h_i} of (43), and outputs the two type collection of a posteriori local error estimates: $\{\eta_{R,K}\}_{K\in\mathcal{T}_{h_i}^i}$ and $\{\eta_{F,K}\}_{K\in\mathcal{T}_{h_i}^i}$. These local error estimates are computed corresponding to the definition outlined in Theorem 2 using the reconstructed equilibrated flux $\boldsymbol{\sigma}_{h_i}$. In accordance with the procedure specified in Definition 4, this equilibrated flux is computed using u_{h_i} and expressed as the sum of local reconstructions (on patches) employing mixed finite element formulations. Such a mixed formulation utilizes hp-adaptive spaces: for a given element $K \in \mathcal{T}_{h_i}^i$, $\mathbf{RT}_{p_K+1}(K)$ is chosen if K is quadrilateral, whereas $\mathbf{BDM}_{p_K+1}(K)$ is employed if K is triangular. The construction of hp-adaptive finite element spaces for mixed formulations is described in Devloo et al. (2016).

5.3 Module MARK

The module MARK receives the benchmark parameters: τ_1, τ_2, ρ; satisfying $0<\tau_2<\tau_1<1$ and $\rho>0$, the tolerance Tol, the prescribed singularity coordinates (when provided) and the collections of a posteriori local error estimates $\{\eta_{R,K}\}_{K\in\mathcal{T}_{h_i}^i}$ and $\{\eta_{F,K}\}_{K\in\mathcal{T}_{h_i}^i}$. It return two disjoint subsets of $\mathcal{T}_{h_i}$, $\mathrm{Ref}H_i$ and $\mathrm{Ref}P_i$, where the first collect the elements that were selected for h-refinement and the second the elements that were selected for p-refinement.

The regularity parameter ρ was introduced inspired by the property indicating that the convergence rate of the data oscillation is higher than that of the flux error Ern and Vohralík (2015).

Algorithm 2: Module Mark

Input: Error estimates $\{\eta_{R,K}\}_{K\in\mathcal{T}_{h_i}^i}$, $\{\eta_{F,K}\}_{K\in\mathcal{T}_{h_i}^i}$; threshold parameters τ_1, τ_2, ρ, Tol

Output: Set of marked elements for h-refinement $\mathrm{Ref}H_i$ and for p-refinement $\mathrm{Ref}P_i$

Set $\mathrm{Ref}H_i := \varnothing$, $\mathrm{Ref}P_i := \varnothing$
forall $K \in \mathcal{T}_h^i$ such that $\eta_{F,K} > Tol$ **do**
  if K has a vertex at the singularity **then**
    Insert K into $\mathrm{Ref}H_i$
  else if $\eta_{F,K} > \tau_1 \max_{K\in\mathcal{T}_h} \eta_{F,K}$ and $\eta_{R,K} > \rho\eta_{F,K}$ **then**
    Insert K into $\mathrm{Ref}H_i$
  else if $\eta_{F,K} < \tau_2 \max_{K\in\mathcal{T}_h} \eta_{F,K}$ or $\eta_{R,K} \le \rho\eta_{F,K}$
    Insert K into $\mathrm{Ref}P_i$
  else
    Element K is not selected for either h-refinement or p-refinement
  end
end

Elements with a singularity at a vertex are prioritized for h-refinement; otherwise, threshold values $\tau_1 = 0.5, \tau_2 = 0.3$, $\rho = 0.05$ and $Tol = 10^{-8}$, are employed to categorize the locally estimated errors within the range

from Tol up to the maximum estimated flux error, $\max_{K\in\mathcal{T}_h}\eta_{F,K}$. Neither h nor p -refinement is performed on mesh elements whose estimated flux errors ($\eta_{F,K}$) are less than Tol. Details are in Algorithm 2.

5.4 Module REFINE

The module REFINE takes as input the disjoint sets of marked elements for h -refinement $\mathrm{Ref}H_i$ and for p -refinement $\mathrm{Ref}P_i$. This one return the mesh $\mathcal{T}_{h_{i+1}}^{i+1}$ and his polynomial-degree distribution $\mathbf{p}_{i+1}$ to be used in the next iteration of the adaptive cycle.

The h -refinement of an element, whether triangular or quadrilateral, involves subdividing it into four sub-elements by pairwise connecting the midpoints of the element edges. Consequently, the children elements are geometrically similar to their parents, therefore, they have the same shape regularity quality as their father.

h -Refinement is applied to each element of $\mathrm{Ref}H_i$. As a result, a new mesh $\mathcal{T}_{h_{i+1}}^{i+1}$ is obtained. In mesh $\mathcal{T}_{h_{i+1}}^{i+1}$ new hanging nodes may appear and/or some hanging nodes of mesh $\mathcal{T}_{h_i}^{i}$ may no longer be hanging nodes of $\mathcal{T}_{h_{i+1}}^{i+1}$.

The p -refinement increases an element's polynomial degree by one. However, for practical purposes, it is well known that a maximum polynomial degree can be set (Mitchell, 2015). In this work, we set this maximum degree to ten. Consequently, an element is p -refined only if its current polynomial degree does not exceed nine. Being $\mathbf{p}_i = (p_K^i)_{K\in\mathcal{T}_{h_i}^i}$ the polynomial degree distribution of the mesh $\mathcal{T}_{h_i}^i$, the polynomial degree distribution $\mathbf{p}_{i+1}$ for the mesh $\mathcal{T}_{h_{i+1}}^{i+1}$ is done as follows: $p_K^{i+1} = p_K^i + 1$ for all $K \in \mathrm{Ref}P_i \cap \mathcal{T}_{h_{i+1}}^{i+1}$ such that $p_K^i \leq 9$, and elements that were not selected for h -refinement or p -refinement retain their polynomial degree. Furthermore, elements obtained by h -refinement preserve the polynomial degree of the parent element.

5.5 Module REGULARIZE

Smoothing of the polynomial degree distribution is performed by increasing by one the polynomial degree of every element that has a neighboring element connected by an edge or part of an edge, whose polynomial degree is greater by two or more. Furthermore, similarly to Demkowicz et al. (1985) and Oliari et al. (2024), mesh smoothing is performed in two steps: (i) Refine all elements with any neighboring element refined twice as much as itself. (ii) Refine all elements surrounded by three or more neighboring elements refined more than itself.

5.6 Sequence of nested hp finite element spaces

Let us recall that, apart from the initial mesh, the meshes produced through the adaptive process are not necessarily conforming, meaning they may contain hanging nodes. The sequence of H^1-conforming finite element spaces $\left(U_{h_i}^{\mathrm{P}_i}\right)_{i\geq 0}$ generated in the hp-adaptive process, forms a nested sequence:

$$U_{h_i}^{\mathrm{P}_i} \subset U_{h_{i+1}}^{\mathrm{P}_{i+1}},\ \forall i \geq 0$$

This nesting property is an extension of the one established for conforming triangular meshes in Daniel et al. (2018). It is fundamentally due to two reasons: (i) the sequence $\left(\mathcal{T}_{h_i}^i\right)_{i\geq 0}$ is hierarchical, meaning that for every $\bar{K} \in \mathcal{T}_{h_{i+1}}^{i+1}$ there exists a unique parent element $K \in \mathcal{T}_{h_i}^i$ such that $\bar{K} \subseteq K$; and (ii) the polynomial degree does not decrease on any element, i.e., for every $\bar{K} \in \mathcal{T}_{h_{i+1}}^{i+1}$ and its corresponding parent element $K \in \mathcal{T}_{h_i}^i$, the inequality $p_K^i \leq p_{\bar{K}}^{i+1}$ holds.

6 NUMERICAL EXPERIMENTATION OF THE hp-ADAPTIVE ALGORITHM PERFORMANCE

This section reports the outcomes of numerical experiments for the hp-adaptive refinement scheme proposed in Section 5. The adaptive process is guided by two types of error estimators, namely the flux estimator and residual estimator, as outlined in Theorem 2, both relying on the flux reconstruction methodology detailed in Section 4.2. Five benchmark problems with known analytical solutions were employed to assess the algorithm's performance, some of these suggested in Mitchell (2013) to test adaptive refinement methods. Additionally, we evaluate the accuracy of the error estimators through the computation of the effectivity index.

6.1. Adaptive process initialization

The benchmark problems chosen for this study are set on either the square domain $\Omega_1 = \left[-1,1\right] \times \left[-1,1\right]$ or the L-shaped domain $\Omega_2 = [-1,1] \times [-1,1] \setminus [0,1] \times [-1,0]$. For every numerical experiment, the initial meshes are designated as $\mathcal{T}_{h_0}$. For problems on the square domain, the adaptive process initiates with a uniform quadrilateral mesh of sixteen square elements or a uniform triangular mesh of thirty-two elements, as can be seen in Figure 4. Similarly, for L-shaped domain problems, uniform initial meshes are employed, as shown in Figure 5.

For each of the five test cases, regardless of mesh type, whether quadrilateral (Quad) or triangular (Tri), the threshold parameters for the hp-adaptivity algorithm were set as follows: $\tau_1 = 0.5$, $\tau_2 = 0.3$, $\rho = 0.05$ and tolerance $Tol = 10^{-8}$. Furthermore, the initial mesh's polynomial degree distribution was uniformly set to one.

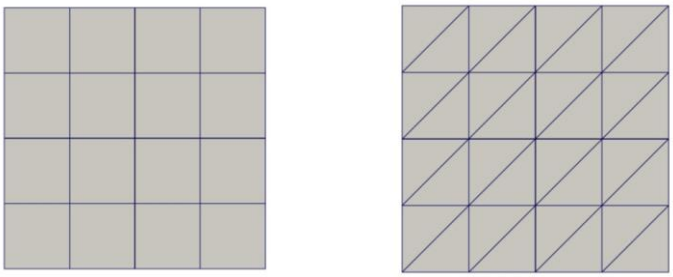

Figure 4. Initial meshes for the domain $\Omega_1 = \left[-1,1\right] \times \left[-1,1\right]$: Uniform quadrilateral mesh (left) and uniform triangular mesh (right).

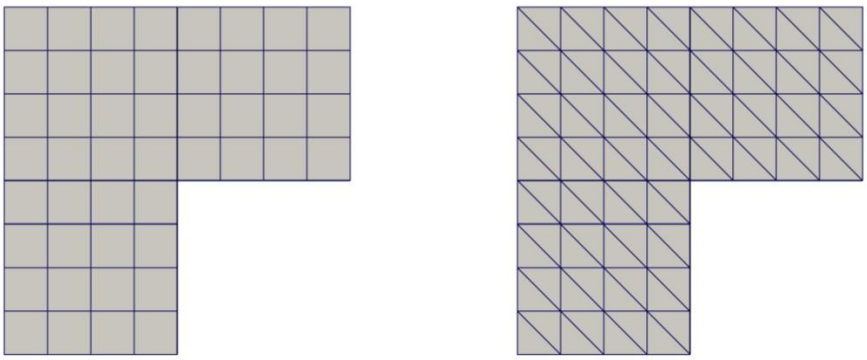

Figure 5. Initial meshes for the L-shaped domain Ω_2 : Uniform quadrilateral mesh (left) and uniform triangular mesh (right).

6.2 Smooth Behavior

Consider the boundary valued problem (1) defined on domain Ω_1, with source term f computed from the exact solution

$$u\left(x,y\right) = \sin\left(\pi x\right)\sin\left(\pi y\right) \tag{44}$$

With A defined as the unitary tensor. This problem has a solution with low variability without abrupt changes, see Figure 6.

This test case is employed to exhibit the numerical behavior of the estimator under a purely p-refinement context, as well as to investigate the hp-adaptive algorithm's performance when h-refinement is unnecessary.

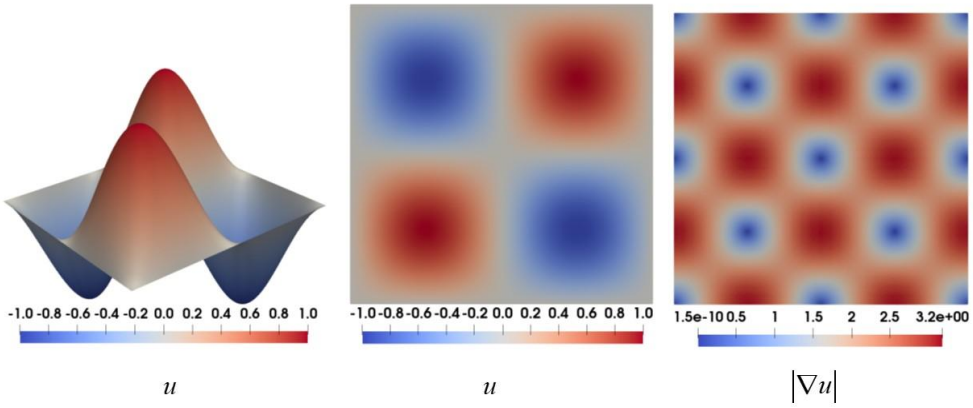

Figure 6. Solution with moderate behavior.

6.2.1 Asymptotic exactness of the error estimator under p-refinement

With the uniform quadrilateral and uniform triangular meshes fixed, as displayed in Figure 4, and an initial polynomial degree distribution uniformly set to one, we applied successive uniform p-refinement until a uniform polynomial degree nine distribution was obtained. Figure 7 illustrates the convergence histories of the energy error and the effectivity index for both mesh types. These results highlight the asymptotic exactness of the error estimator when subjected to uniform p-refinement.

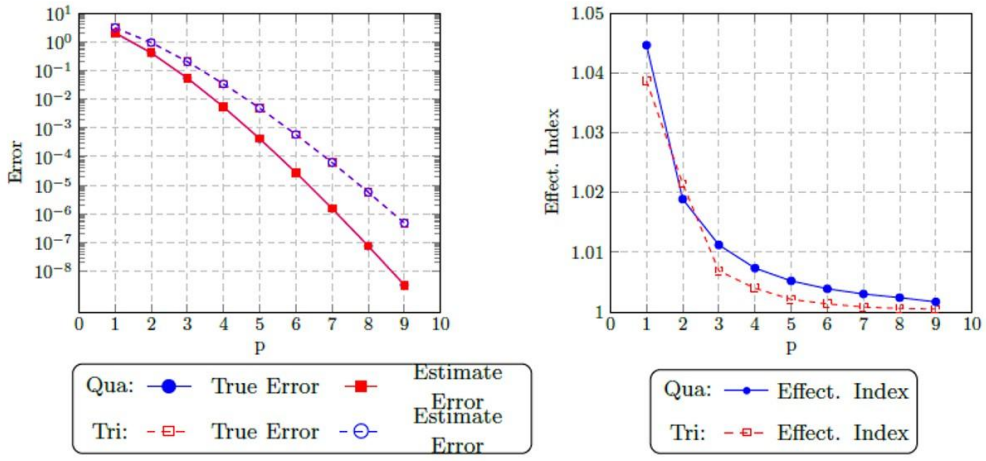

Figure 7. Problem with solution of moderate behavior: Evolution of the true error (left) and effectivity index (right) under uniform p-refinement with a fixed mesh.

6.2.2 hp-Adaptivity for the problem with solution of smooth behavior

Figure 8 displays the results of applying the adaptive algorithm to solve the problem with a smooth analytical solution, using both quadrilateral and triangular meshes. For both mesh configurations, the initial mesh, initial polynomial degree distribution, and adaptive algorithm parameter values were detailed in Section 6.1.

The adaptive algorithm identified that h-refinement was not required, and during each iteration, was performed only p-refinement on all mesh elements, leading to a final geometric mesh identical to the initial one, and yielding a final polynomial degree distribution uniformly set to 9. In Figure 8, the convergence histories of the hp-adaptive scheme (nine iterations) are contrasted with those of uniform h-refinement under constant polynomial orders $p=1$ and $p=2$, including their respective effectivity indices.

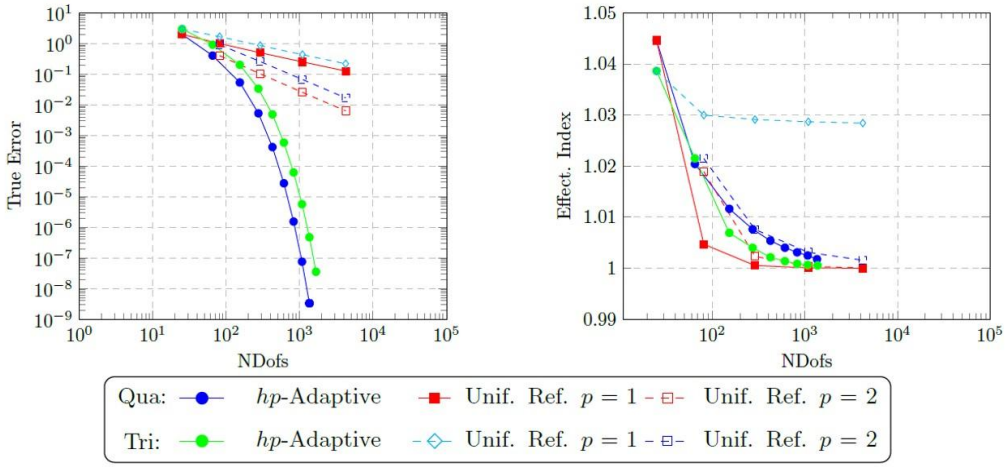

Figure 8. Problem with moderate behavior solution: Convergence performance under hp-adaptivity scheme in contrast to uniform h-refinement with fixed polynomial degrees $p=1$ and $p=2$ (left), and the corresponding effectivity indices (right).

6.3. Sharp Gaussian

Consider the boundary valued problem (1) on domain Ω_1, where A represents the unitary tensor and the source term f is computed from the exact solution

$$u(x,y)=\left(x^2-1\right)\left(y^2-1\right)e^{-1000\left(x^2+y^2\right)} \tag{45}$$

The solution to the problem is smooth, but presents a sharp peak in the center of the domain, see Figure 9.

This problem is used to exhibit the ability of the hp-adaptive algorithm to detect and concentrate h-refinement in small regions where abrupt variations occur, as well as to demonstrate the ability to properly alternate between h and p-refinement.

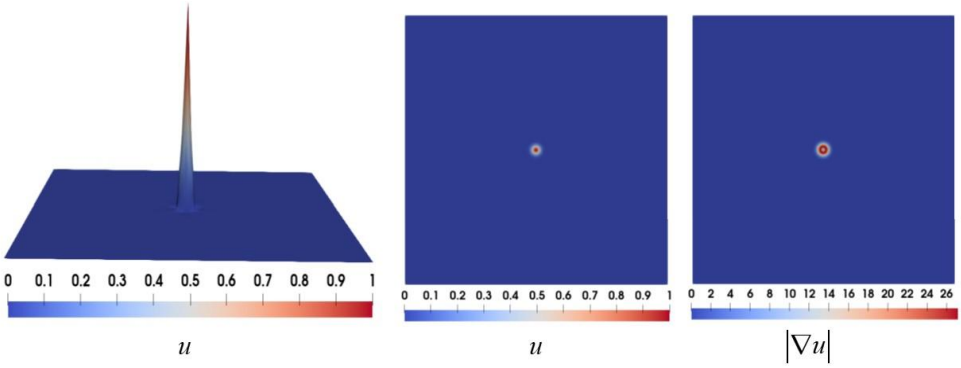

Figure 9. Solution with a peak.

6.3.1. hp-Adaptivity for the problem with solution featuring a sharp peak

The adaptive process was initiated with the configuration specified in Section 6.1 Throughout the 14 iterations of the adaptive process, the hp-adaptive algorithm effectively alternated between h-refinement and p-refinement, thereby attaining optimal convergence behavior. In Figure 10, the convergence histories of the hp-adaptive scheme are contrasted with those of uniform h-refinement under constant polynomial orders $p=1$ and $p=2$, including their respective effectivity indices. Figure 11 shows the distribution, by element, of the estimated flux errors for meshes $\mathcal{T}_h^2$, $\mathcal{T}_h^6$ and $\mathcal{T}_h^{11}$. Figure 12 shows the distribution of polynomial degrees for the aforementioned meshes.

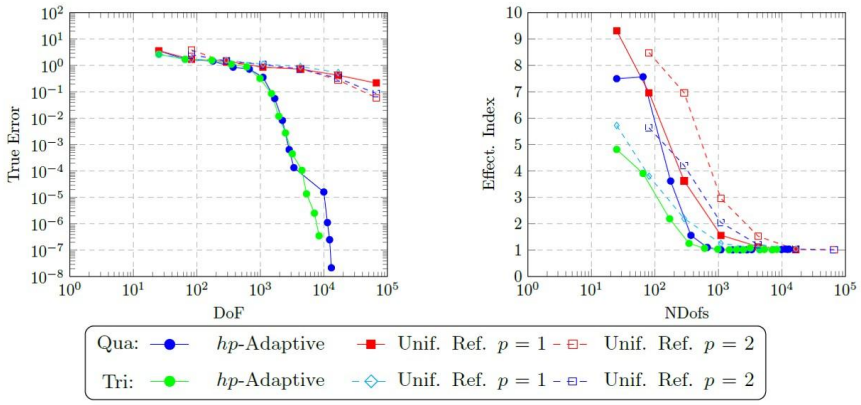

Figure 10. Problem with an analytical solution featuring a sharp peak: Convergence performance under hp -adaptivity scheme in contrast to uniform h -refinement with fixed polynomial degrees $p=1$ and $p=2$ (left), and the corresponding effectivity indices (right).

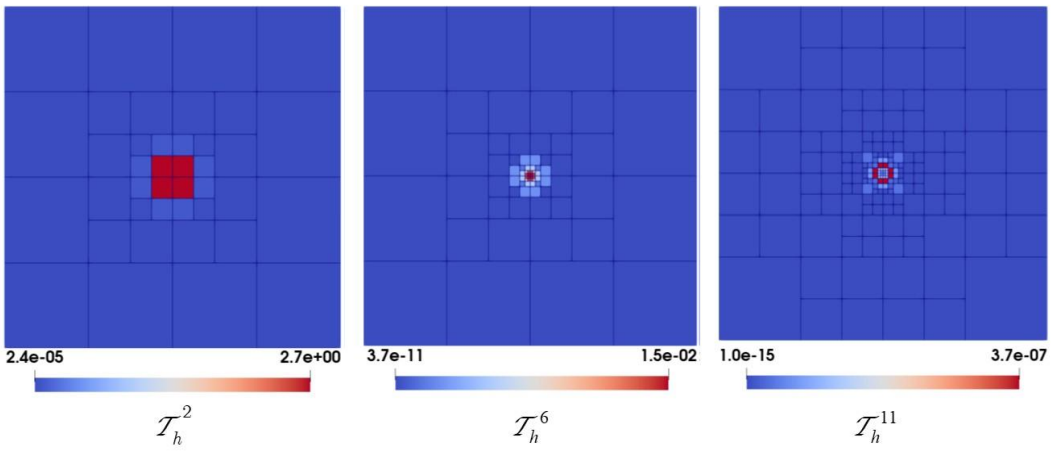

Figure 11. hp -Adaptivity for problem with an analytical solution featuring a peak: Distribution of the estimated flux error by element, for the meshes $\mathcal{T}_h^2$, $\mathcal{T}_h^6$ and $\mathcal{T}_h^{11}$.

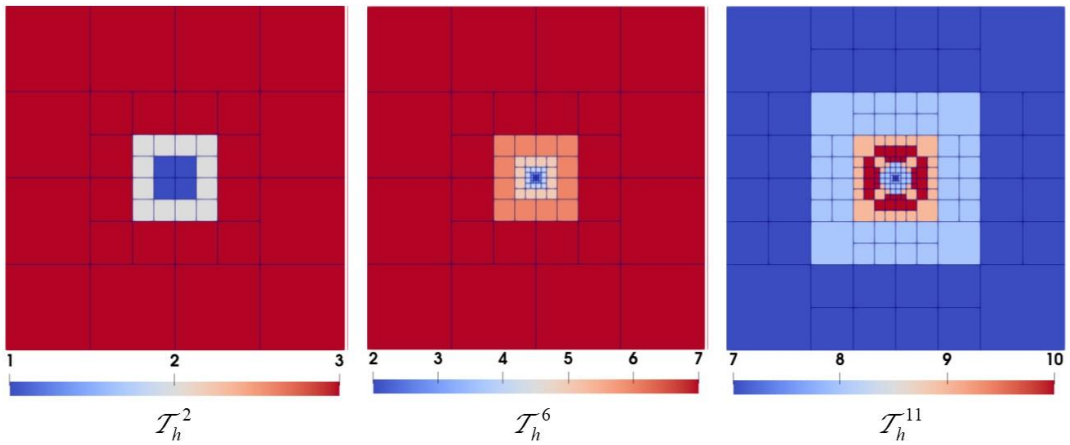

Figure 12. hp -Adaptivity for problem with a solution featuring a peak: Polynomial degree distribution for the meshes $\mathcal{T}_h^2$, $\mathcal{T}_h^6$ and $\mathcal{T}_h^{11}$.

6.4. Steep wave

Consider the boundary valued problem (1) on domain Ω_1, with A defined as the unitary tensor and the source term f is computed from the exact solution

$$u\left(x,y\right)=0.4\left(1-x^2\right)\left(1-y^2\right)\left(\frac{\pi}{2}+\arctan\left(5\left(3-10\left(x^2+y^2\right)\right)\right)\right) \tag{46}$$

The solution to the problem presents high gradients on a circumference centered on the origin of the coordinates, see Figure 13.

This problem is used to exhibit the ability of the hp-adaptive algorithm to detect high gradients over a curve and concentrate h-refinement in the surroundings of this curve, as well as to demonstrate the ability to properly alternate between h and p refinement.

6.4.1 hp-Adaptivity for the problem with solution featuring high gradients

With the hp-adaptive process startup configuration set as described in Section 6.1. During the 14-step iterative procedure, the hp-adaptive algorithm dynamically selected between h and p-refinement based on local error indicators, resulting in optimal convergence characteristic. In Figure 14, we contrast the convergence histories of the hp-adaptive scheme with those of uniform h-refinement under constant polynomial orders $(p=1$ and $p=2)$, including their respective effectivity indices. Figure 15 shows the distribution, by element, of the estimated flux errors for meshes $\mathcal{T}_h^2$, $\mathcal{T}_h^6$ and $\mathcal{T}_h^{11}$. Figure 16 shows the distribution of polynomial degrees for the aforementioned meshes.

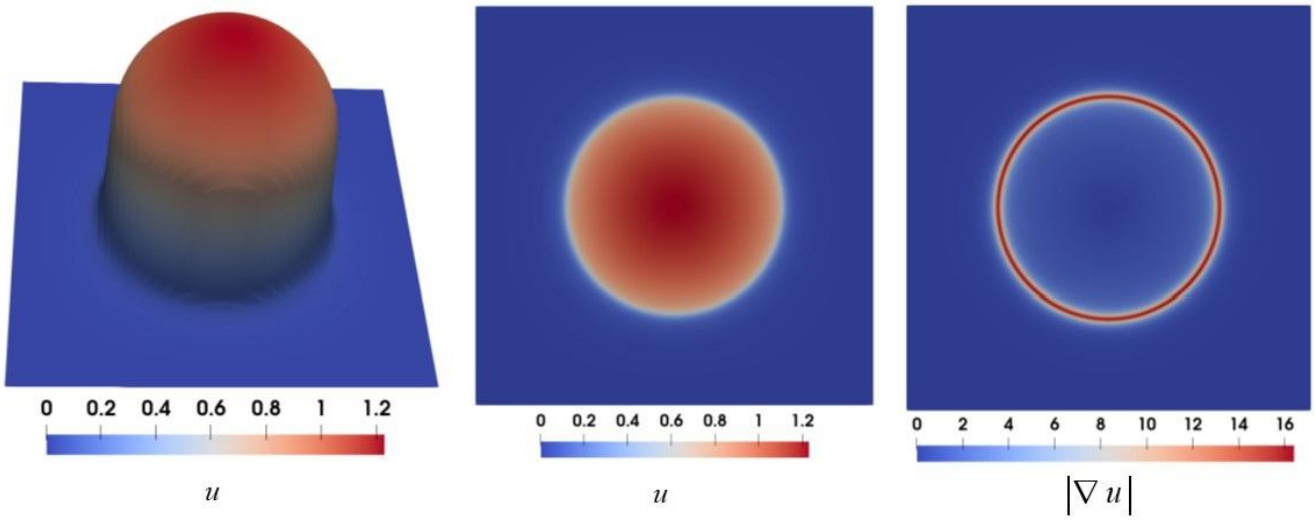

Figure 13. Solution featuring high gradients.

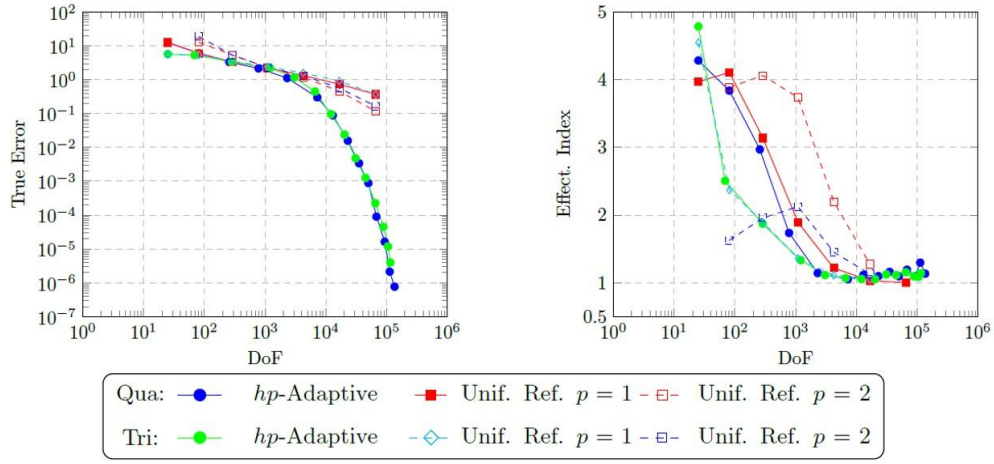

Figure 14. hp -Adaptivity for the problem with an solution featuring high gradients: Convergence performance under hp -adaptivity scheme in contrast to uniform h -refinement with fixed polynomial degrees $p=1$ and $p=2$ (left), and the corresponding effectivity indices (right).

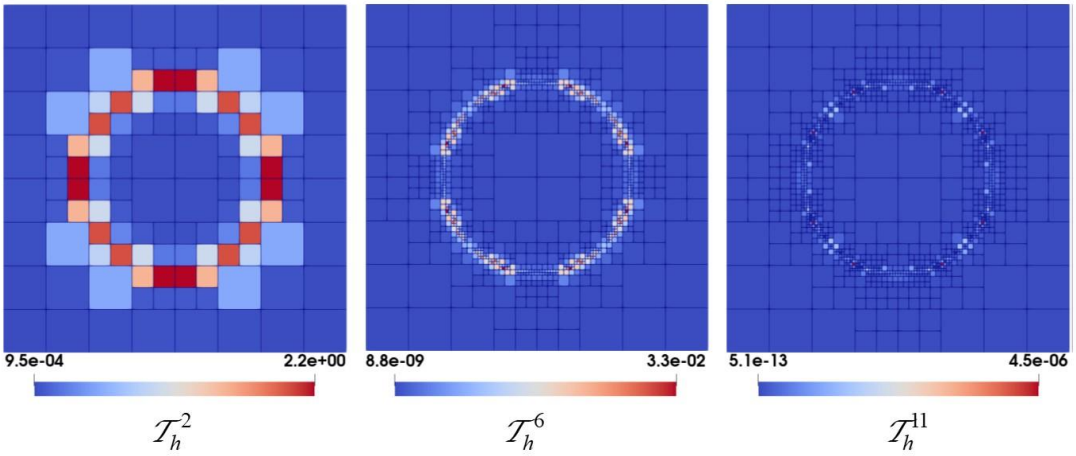

Figure 15. hp -Adaptivity for the problem with solution featuring high gradients: Distribution of the estimated flux error by element, for the meshes $\mathcal{T}_h^2$, $\mathcal{T}_h^6$ and $\mathcal{T}_h^{11}$.

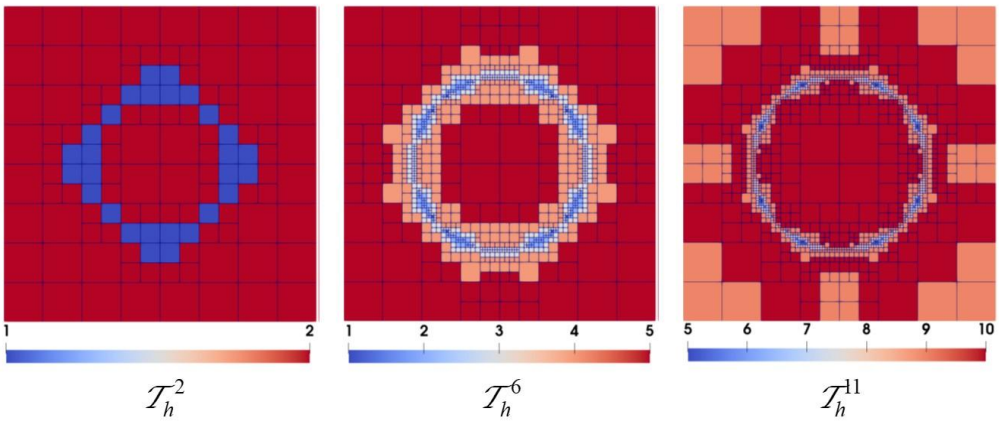

Figure 16. hp -Adaptivity for the problem with solution featuring high gradients: Polynomial degree distribution for the meshes $\mathcal{T}_h^2$, $\mathcal{T}_h^6$ and $\mathcal{T}_h^{11}$.

6.5. Reentrant corner singularity

Consider the boundary valued problem (1) on domain Ω_2, where A is the unitary tensor and the source term f is computed from the exact solution

$$u\left(x,y\right)=\cos\left(\frac{\pi x}{2}\right)\cos\left(\frac{\pi y}{2}\right)r^{2/3}\ \sin\left(\frac{2\arctan\left(y/x\right)}{3}\right) \tag{47}$$

The solution to this problem display a singularity in the reentrant corner of its L-shaped domain, see Figure 17.

We selected this benchmark problem to show the hp-adaptive algorithm's performance in the presence of prescribed points of singularities and to test the estimator's accuracy.

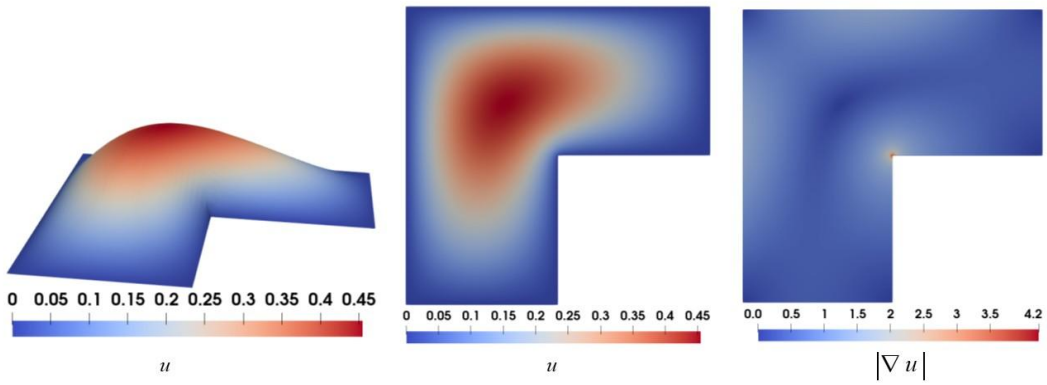

Figure 17. Solution with a singularity in the reentrant corner.

6.5.1 hp-Adaptivity for the problem whose solution presents singularity in the reentrant corner

With the adaptive process startup configuration set as described in Section 6.1. Throughout the 14 iterations of the adaptive process, the hp-adaptive algorithm effectively alternated between h-refinement and p-refinement, resulting in optimal convergence characteristics. In Figure 18, we contrast the convergence histories of the hp-adaptive scheme with those of uniform h-refinement under constant polynomial orders $(p=1 \text{ and } p=2)$, including their respective effectivity indices. Figure 19 shows the distribution, by element, of the estimated flux errors for meshes $\mathcal{I}_h^2$, $\mathcal{I}_h^6$ and $\mathcal{I}_h^{11}$. Figure 20 shows the distribution of polynomial degrees for the aforementioned meshes.

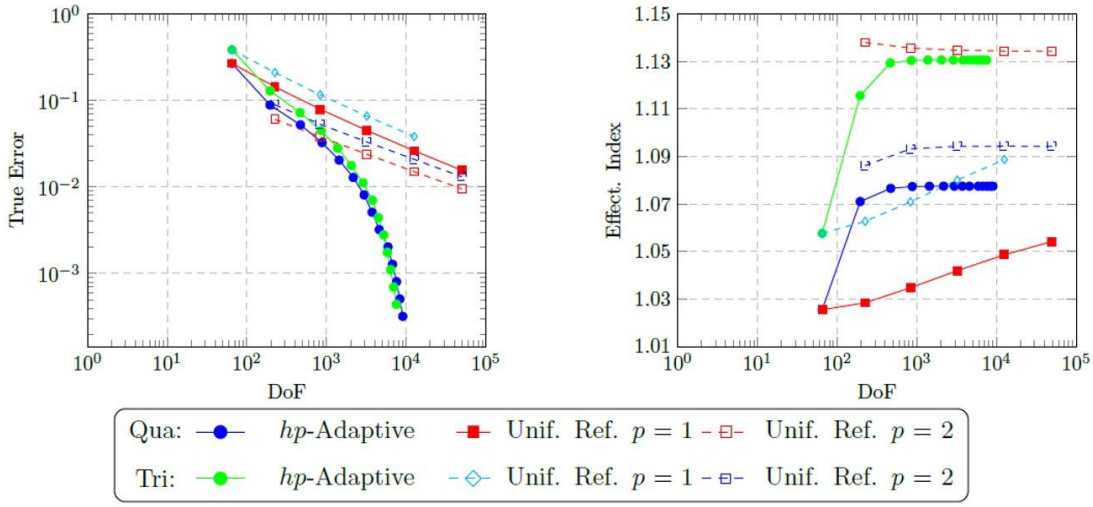

Figure 18. hp -Adaptivity for the problem with solution featuring a singularity: Convergence performance under adaptivity scheme in contrast to uniform h -refinement with fixed polynomial degrees $p=1$ and $p=2$ (left), and the corresponding effectivity indices (right).

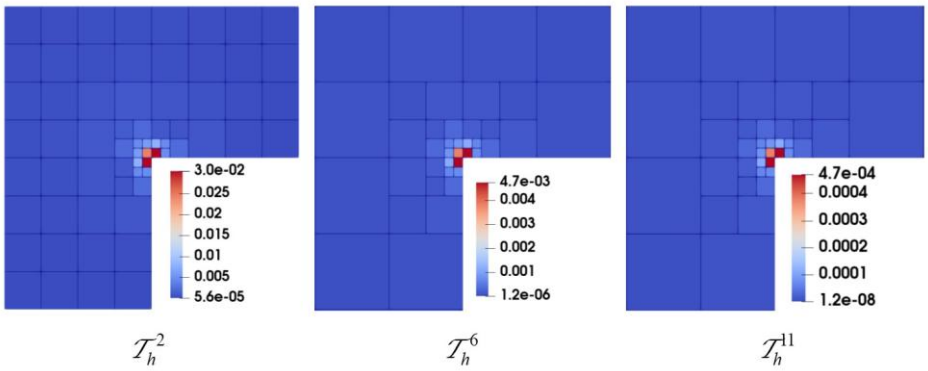

Figure 19. hp -Adaptivity for the problem with an analytical solution featuring a singularity: Distribution of the estimated flux error by element, for the meshes $\mathcal{T}_h^2$, $\mathcal{T}_h^6$ and $\mathcal{T}_h^{11}$. Meshes $\mathcal{T}_h^6$ and $\mathcal{T}_h^{11}$ are shown zoomed around the singularity, on $\left[-\frac{1}{16},\frac{1}{16}\right]\times\left[-\frac{1}{16},\frac{1}{16}\right]\setminus\left[0,\frac{1}{16}\right]$ and $\left[\frac{-1}{512},\frac{1}{512}\right]\times\left[\frac{-1}{512},\frac{1}{512}\right]\setminus\left[\frac{-1}{512},0\right]$ respectively.

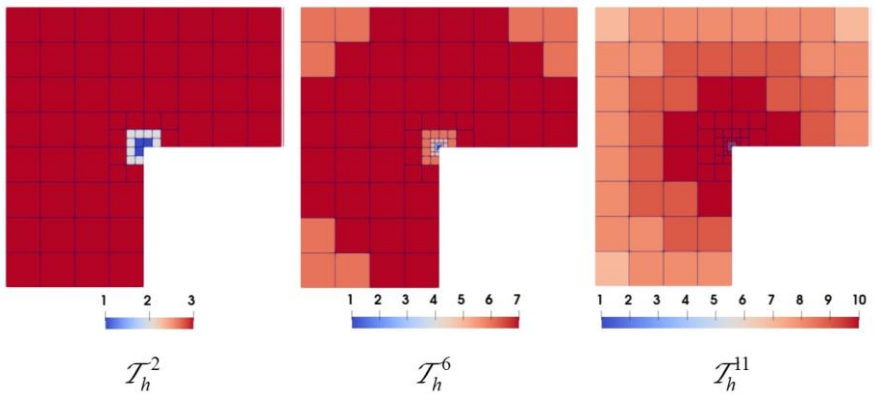

Figure 20. hp -Adaptivity for the problem with an analytical solution featuring a singularity: Distribution of the polynomial order p per element for the meshes $\mathcal{T}_h^2$, $\mathcal{T}_h^6$ and $\mathcal{T}_h^{11}$.

6.6. Contrasting permeability

Consider the boundary valued problem (1) on Ω_1. In this case, A is a piecewise constant permeability tensor

$$A=\begin{cases}5I & \text{for } x,y\leq 0 \text{ or } x,y\geq 0\\ I & \text{otherwise}\end{cases} \tag{48}$$

and the source term f is computed from the exact solution

$$u(x,y)=\cos\left(\frac{\pi x}{2}\right)\cos\left(\frac{\pi y}{2}\right)r^{\lambda}\left(\alpha\cos(\lambda\theta)+\beta\sin(\lambda\theta)\right) \tag{49}$$

where $\lambda=0.53544094560246$ and,

$$\left(\alpha,\beta\right)=\begin{cases}\left(1.0000000000000000,0.44721359549995787\right) & x\in\left[0,1\right]\times\left[0,1\right]\\ \left(2.3333333333333326,-0.7453559924999296\right) & x\in\left[-1,0\right)\times\left(0,1\right]\\ \left(0.5555555555555556,-0.9441175904999111\right), & x\in\left[-1,0\right]\times\left[-1,0\right]\\ \left(-0.48148148148148173,-2.4017026424997736\right) & x\in\left(0,1\right]\times\left[-1,0\right)\end{cases} \tag{50}$$

We use this problem to assess the error estimator's accuracy and the hp-adaptive algorithm's performance in a context featuring a discontinuous permeability tensor and prescribed solution singularities.

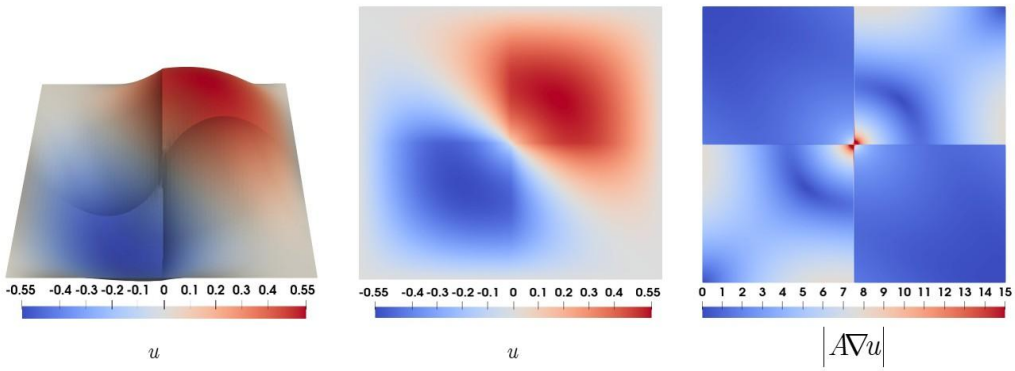

Figure 21. Solution of the problem with contrasting permeability.

6.6.1 hp-Adaptivity for the problem with contrasting permeability

The startup configuration for the adaptive process followed Section 6.1. Throughout the 14 iterations of the adaptive process, the hp-adaptive algorithm effectively alternated between h-refinement and p-refinement, thereby attaining optimal convergence behavior. We observe that, even though the adaptive meshes exhibit approximations with exponential convergence, the effectivity index does not converge to 1, see Figure 22 (right). It is the best result we could obtain for the presented reconstruction algorithm.

Figure 22 contrast the convergence histories of the hp-adaptive scheme with those of uniform h-refinement under constant polynomial orders $p=1$ and $p=2$, with accompanying effectivity indices (right). Figure 23 shows the distribution, by element, of the estimated flux errors for meshes $\mathcal{T}_h^2$, $\mathcal{T}_h^6$ and $\mathcal{T}_h^{11}$. Figure 24 shows the distribution of polynomial degrees for the aforementioned meshes.

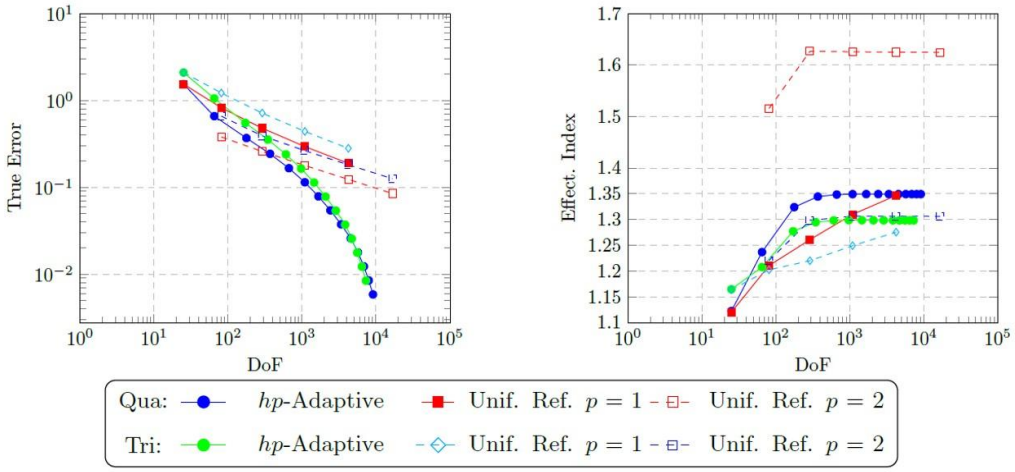

Figure 22. hp -Adaptivity for the problem with contrasting permeability: Convergence performance under hp - adaptivity scheme in contrast to uniform h -refinement with fixed polynomial degrees $p = 1$ and $p=2$ (left), and the corresponding effectivity indices (right).

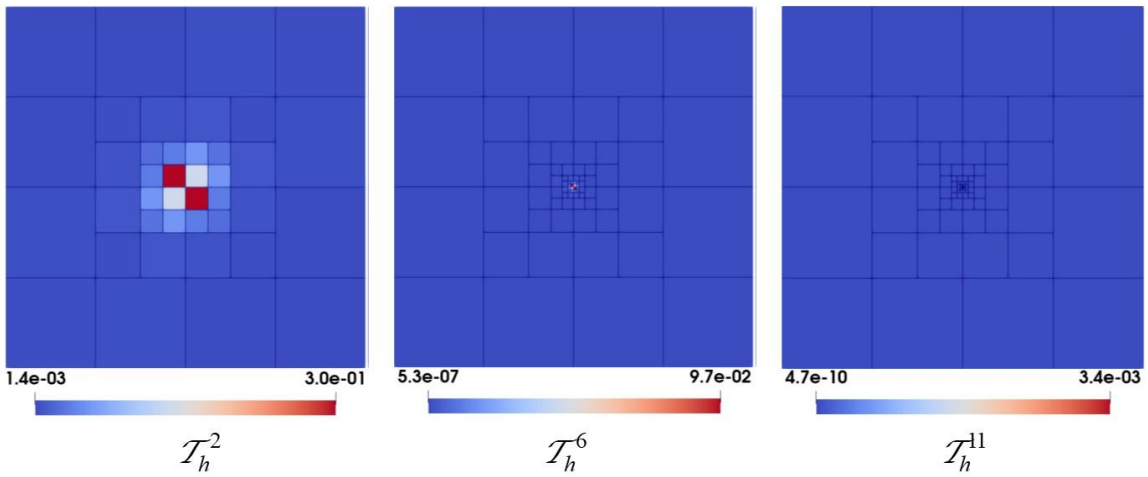

Figure 23. hp -Adaptivity for the problem with contrasting permeability: Distribution of the estimated flux error by element, for the meshes $\mathcal{T}_h^2$, $\mathcal{T}_h^6$ and $\mathcal{T}_h^{11}$.

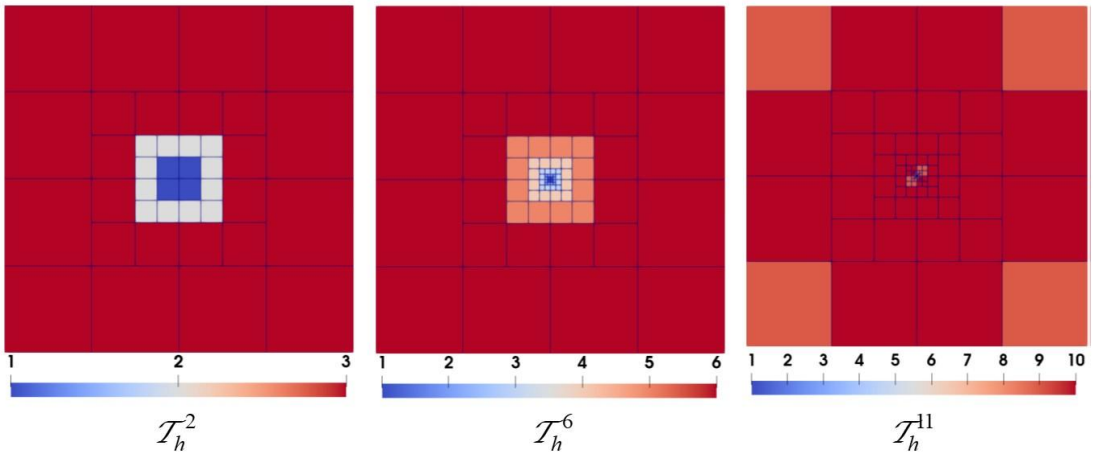

Figure 24. hp -Adaptivity for the problem with contrasting permeability: Distribution of the polynomial order p for the meshes $\mathcal{T}_h^2$, $\mathcal{T}_h^6$ and $\mathcal{T}_h^{11}$.

7 DEPENDENCE ON PARAMETER VARIATIONS

To assess the sensitivity of the hp-adaptive refinement strategy to the parameters τ_1, τ_2 and ρ, a total of nine numerical experiments were performed for each of the five model problems, The parameter values were systematically adjusted around the threshold values established in Section 6, as follows: $\tau_1 \in \{0.4, 0.6\}$, $\tau_2 \in \{0.2, 0.4\}$, and $p \in \{0.03, 0.07\}$. The results for the problem with a solution characterized by steep gradients concentrated along a circumference are shown in Figure 25. For the remaining model problems that were used in the Section 6, the convergence history and effectivity index plots demonstrated an even weaker dependence on parameter variations.

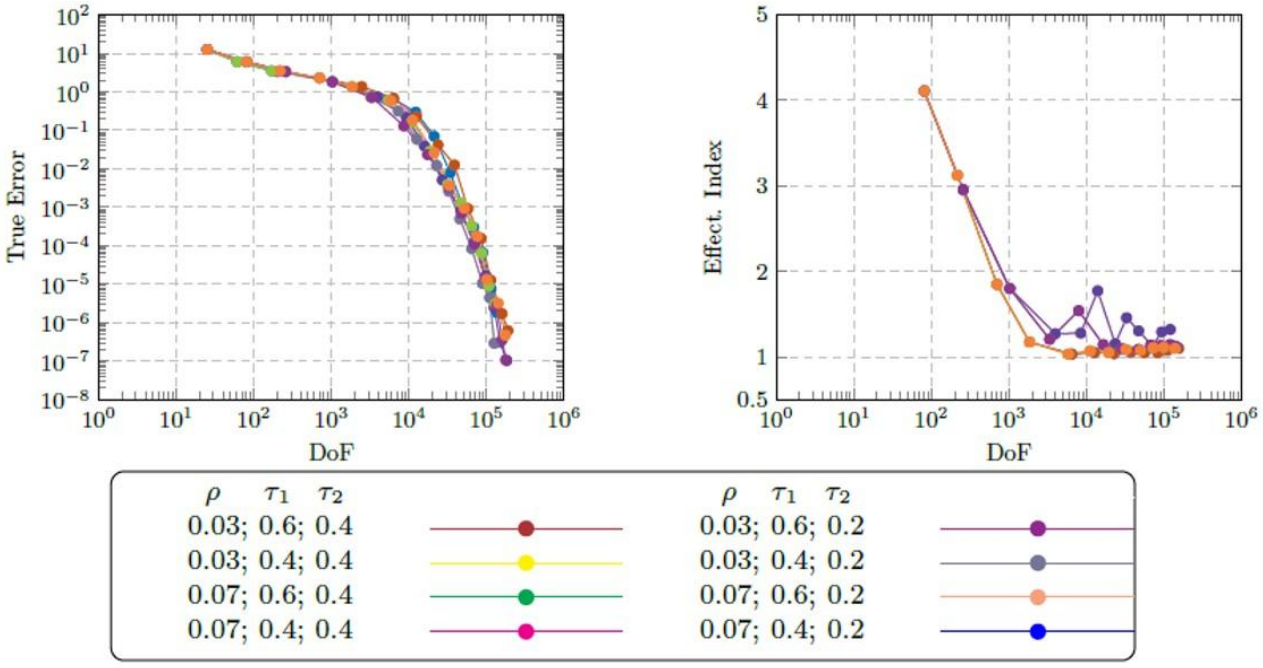

Figure 25. Parameter sweep for the problem with solution featuring high gradients.

The results of the sensitivity experiments conducted show that the adaptive refinement strategy, guided by the error estimator, exhibits consistency across different parameter values, ensuring its reliability without requiring fine-tuned parameter adjustments.

8 CONCLUSIONS

In this work an innovative hp-adaptive strategy is presented based on an a-posteriori error estimator derived from the Prager Synge theorem. The estimated error of each element is composed of two contributions: one error derived from the reconstructed flux and a second error due to the error of the divergence of the flux. Where the flux error and divergence error dominate, h-adaptivity is applied; otherwise, if either of these is low, p-adaptivity is chosen. The adaptive strategy is applied to a variety of numerical problems, demonstrating its robustness. In all problems that were studied exponential convergence was observed as a function of the number of degrees of freedom.

The flux reconstruction is based on a local reconstruction. The reconstruction formulation has been extended to heterogeneous permeability. Also, the partition of unity function required for such reconstruction is built using the h-irregular mesh.

Acknowledgments

The authors are grateful for the financial support subsidized, with contract number IBAIB-03-2019-UNSA, by the “Universidad Nacional de San Agustin de Arequipa, Perú”.

Author's Contribuitions: Conceptualization, Philippe R. B. Devloo, Ricardo J. Hancco Ancori; Formal Analysis, Philippe R. B. Devloo, Ricardo J. Hancco Ancori, Eliseo D. Velasquez Condori, Roger E. Mestas Chavez, Fermín F. Mamani Condori; Funding Acquisition, Ricardo J. Hancco Ancori; Investigation, Ricardo J. Hancco Ancori, Eliseo D. Velásquez Condori, Roger E. Mestas Chavez, Fermín F. Mamani Condori; Project Administration, Roger E. Mestas Chavez, Fermín F. Mamani Condori; Software, Philippe R. B. 425 Devloo, Ricardo J. Hancco Ancori, Eliseo D. Velásquez Condori; Supervision, Philippe R. B. Devloo; Writing - Original Draft, Ricardo J. Hancco Ancori; Writing - Review & Editing, Philippe R. B. Devloo, Eliseo D. Velásquez Condori.

Data availability statement: Research data is only available upon request.

Editor: Marco L. Bittencourt

References

Ainsworth, M., Oden, J.T., 2011. A Posteriori Error Estimation in Finite Element Analysis. John Wiley & Sons.

Ainsworth, M., Senior, B., 1998. An adaptive refinement strategy for hp-finite element computations. Applied Numerical Mathematics 26, 165-178.

Ainsworth, M., Senior, B., 1999. hp-finite element procedures on non-uniform geometric meshes: Adaptivity and constrained approximation, in: Grid Generation and Adaptive Algorithms. Springer, pp. 1-27.

Becker, R., Bordas, S.P., Chouly, F., Omnes, P., 2024. A short perspective on a posteriori error control and adaptive discretizations. Advances in Applied Mechanics 58, 1-36.

Bertrand, F., Boffi, D., et al., 2020. The prager-synge theorem in reconstruction based a posteriori error estimation. CONTEMPORARY MATHEMATICS 754, 45-67.

Braess, D., Pillwein, V., Schoberl, J., 2009. Equilibrated residual error estimates are p-robust. Computer Methods in Applied Mechanics and Engineering 198, 1189-1197.

Bringmann, P., Mirad, A., Praetorius, D., 2024. Iterative solvers in adaptive fem: Adaptivity yields quasi- optimal computational runtime. Advances in Applied Mechanics 59, 147-212.

Chamoin, L., Legoll, F., 2023. An introductory review on a posteriori error estimation in finite element computations. SIAM Review 65, 963-1028.

Daniel, P., Ern, A., Smears, I., Vohralík, M., 2018. An adaptive hp-refinement strategy with computable guaranteed bound on the error reduction factor. Computers & Mathematics with Applications 76, 967-983.

De Siqueira, D., Devloo, P.R., Gomes, S.M., 2013. A new procedure for the construction of hierarchical high order hdiv and hcurl finite element spaces. Journal of Computational and Applied Mathematics 240, 204-214.

Demkowicz, L., Devloo, P., Oden, J.T., 1985. On an h-type mesh-refinement strategy based on minimization of interpolation errors. Computer Methods in Applied Mechanics and Engineering 53, 67-89.

Demkowicz, L., Rachowicz, W., Devloo, P., 2002. A fully automatic hp-adaptivity. Journal of Scientific Computing 17, 117-142.

Devloo, P.R., Farias, A.M., Gomes, S.M., de Siqueira, D., 2016. Two-dimensional hp adaptive finite element spaces for mixed formulations. Mathematics and Computers in Simulation 126, 104-122.

Devloo, P.R.B., 1997. Pz: An object oriented environment for scientific programming. Computer methods in applied mechanics and engineering 150, 133-153.

Dolejsi, V., Ern, A., Vohralík, M., 2016. hp-adaptation driven by polynomial-degree-robust a posteriori error estimates for elliptic problems. SIAM Journal on Scientific Computing 38, A3220-A3246.

Dorfler, W., Heuveline, V., 2007. Convergence of an adaptive hp finite element strategy in one space dimension. Applied numerical mathematics 57, 1108-1124.

Eibner, T., Melenk, J.M., 2007. An adaptive strategy for hp-fem based on testing for analyticity. Computational Mechanics 39, 575-595.

Ern, A., Vohralík, M., 2015. Polynomial-degree-robust a posteriori estimates in a unified setting for conforming, nonconforming, discontinuous galerkin, and mixed discretizations. SIAM Journal on Numerical Analysis 53, 1058-1081.

Ervin, V., 2012. Computational bases for rtk and bdmk on triangles. Computers & Mathematics with Applications 64, 2765-2774.

Farias, A.M., Devloo, P.R., Gomes, S.M., de Siqueira, D., Castro, D.A., 2017. Two dimensional mixed finite element approximations for elliptic problems with enhanced accuracy for the potential and flux divergence. Computers & Mathematics with Applications 74, 3283-3295.

Gui, W.z., Babuska, I., 1986. The h, p and hp versions of the finite element method in 1 dimensión: Part i. the error analysis of the p-version, part ii. the error analysis of the h- and *h*-*p*-versions, part iii. The adaptive *h*-*p* version. Numerische Mathematik 49, 577-683.

Guo, B., Babuska, I., 1986a. The hp version of the finite element method: Part 1: The basic approximation results. Computational Mechanics 1, 21-41.

Guo, B., Babuska, I., 1986b. The hp version of the finite element method: Part 2: General results and applications. Computational Mechanics 1, 203-220.

Heuveline, V., Rannacher, R., 2003. Duality-based adaptivity in the hp-finite element method. Journal of Numerical Mathematics 11, 95-113.

Houston, P., Süli, E., 2005. A note on the design of hp-adaptive finite element methods for elliptic partial differential equations. Computer Methods in Applied Mechanics and Engineering 194, 229-243.

Ladeveze, P., Leguillon, D., 1983. Error estimate procedure in the finite element method and applications. SIAM Journal on Numerical Analysis 20, 485-509.

Melenk, J.M., Wohlmuth, B.I., 2001. On residual-based a posteriori error estimation in hp-fem. Advances in Computational Mathematics 15, 311-331.

Mitchell, W.F., 2013. A collection of 2d elliptic problems for testing adaptive grid refinement algorithms. Applied mathematics and computation 220, 350-364.

Mitchell, W.F., 2015. How high a degree is high enough for high order finite elements? Procedia Computer Science 51, 246-255.

Mitchell, W.F., McClain, M.A., 2011. A survey of hp-adaptive strategies for elliptic partial differential 500 equations, in: Recent advances in computational and applied mathematics, Springer. pp. 227-258.

Mitchell, W.F., McClain, M.A., 2014. A comparison of hp-adaptive strategies for elliptic partial differential equations. ACM Transactions on Mathematical Software (TOMS) 41, 1-39.

Oliari, V.B., Bosing, P.R., de Siqueira, D., Devloo, P.R., 2024. A posteriori error estimates for primal hybrid finite element methods applied to poisson problem. Journal of Computational and Applied Mathematics 441, 115671.

Prager, W., Synge, J.L., 1947. Approximations in elasticity based on the concept of function space. Quarterly of Applied Mathematics 5, 241-269.

Rachowicz, W., Pardo, D., Demkowicz, L., 2006. Fully automatic hp-adaptivity in three dimensions. Computer methods in applied mechanics and engineering 195, 4816-4842.

Synge, J.L., 1957. The hypercircle in mathematical physics. Cambridge University Press Cambridge.

Verfürth, R., 2013. A posteriori error estimation techniques for finite element methods. OUP Oxford.